SCDNA: a serially complete precipitation and temperature dataset for North America from 1979 to 2018

Guoqiang Tang[1,2], Martyn P. Clark[1,2], Andrew J. Newman[3], Andrew W. Wood[3], Simon Michael Papalexiou[2,4], Vincent Vionnet[5], and Paul H. Whitfield[1,2]

[1]University of Saskatchewan Coldwater Lab, Canmore, Alberta, Canada

[2]Centre for Hydrology, University of Saskatchewan, Saskatoon, Saskatchewan, Canada

[3]National Center for Atmospheric Research, Boulder, Colorado

[4]Department of Civil, Geological and Environmental Engineering, University of Saskatchewan, Saskatchewan, Canada

[5]Environmental Numerical Research Prediction, Environment and Climate Change Canada, Dorval, Quebec, Canada

Correspondence to: Guoqiang Tang (guoqiang.tang@usask.ca)

Abstract: Station-based serially complete datasets (SCDs) of precipitation and temperature observations are important for hydrometeorological studies. Motivated by the lack of serially-complete station observations for North America, this study seeks to develop a SCD from 1979 to 2018 from station data. The new SCD for North America (SCDNA) includes daily precipitation, minimum temperature (T_{min}), and maximum temperature (T_{max}) data for 27276 stations. Raw meteorological station data were obtained from the Global Historical Climate Network Daily (GHCN-D), the Global Surface Summary of the Day (GSOD), Environment and Climate Change Canada (ECCC), and a compiled station database in Mexico. Stations with at least 8-year records were selected, which underwent location correction and were subjected to strict quality control. Outputs from three reanalysis products (ERA5, JRA-55, and MERRA-2) provided auxiliary information to estimate station records. Infilling during the observation period and reconstruction beyond the observation period were accomplished by combining estimates from 16 strategies (variants of quantile mapping, spatial interpolation, and machine learning). A sensitivity experiment was conducted by assuming 30% observations of stations were missing – this enabled independent validation and provided a reference for reconstruction. Quantile mapping and mean-value corrections were applied to the final estimates. The median Kling-Gupta efficiency (KGE') values of the final SCDNA for all stations are 0.90, 0.98, and 0.99 for precipitation, T_{min} and T_{max}, respectively. The SCDNA is closer to station observations than the four benchmark gridded products, and can be used in applications that require either quality-controlled meteorological station observations or reconstructed long-term estimates for analysis and modelling. The dataset is available at https://doi.org/10.5281/zenodo.3735533 (Tang et al., 2020).

Key words: serially complete dataset; precipitation; temperature; North America

1 Introduction

Station-based serially complete datasets (SCDs, see Table A1 for all acronyms) are important for meteorological, climatological and hydrological studies (Kanda et al., 2018; Ramos‑Calzado et al., 2008), such as producing retrospective gridded products (Di Luzio et al., 2008; Kenawy et al., 2013; Newman et al., 2019; Serrano-Notivoli et al., 2019), trend analyses (Knowles et al., 2006; Anderson et al., 2009; Papalexiou and Montanari, 2019), and climatologic index calculation (Alexander et al., 2006; Papalexiou et al., 2018). These SCDs are useful because station-based observational datasets often contain missing values due to factors such as observer absence, instrument failures, and interrupted communication (Hasanpour Kashani and Dinpashoh, 2012). Moreover, station observations failing quality control tests such as outlier and homogeneity checks may not be reliable (Menne et al., 2012), and many stations are only maintained over a relatively short period of time or portions of the year, resulting in data gaps that could affect the analysis of climate variability or long-term trends (Rubin, 1976; Stooksbury et al., 1999). Serial completeness is also a critical requirement for real-time station-based applications, which regularly contend with missing data values due to latencies in station reporting, quality control and processing (Tang et al., 2009).

Many methods have been developed to estimate missing observations and reconstruct time series of meteorological stations that provide point-scale regular observations of atmospheric conditions (Longman et al., 2020). They can be classified as self-contained infilling, spatial interpolation, quantile mapping, and machine learning methods.

1. Self-contained infilling only uses records from the target station to estimate its own missing values. Typical methods include interpolation based on data from previous and subsequent days or replacing missing values by long-term mean (Kemp et al., 1983; Pappas et al., 2014). Self-contained infilling, however, only performs well for variables with high temporal autocorrelation such as temperature and is problematic for daily precipitation (Simolo et al., 2010; Teegavarapu and Chandramouli, 2005), and in covering lengthy data gaps.

2. Spatial interpolation uses neighboring stations (identified on spatial distance or statistical similarity) to estimate data at the target station. Spatial interpolation methods can be divided into two types: the first uses information only from neighboring stations; and common methods include linear interpolation and inverse distance weighting (IDW; Shepard, 1968). The second method needs information from both neighboring and target stations. Typical examples include the revised normal ratio (NR; Young, 1992) and the single best estimator (Eischeid et al., 1995, 2000), both of which use correlation coefficients (CCs) between target and neighboring stations to estimate merging weights. This second type of spatial interpolation also includes more sophisticated methods (e.g., multiple linear regression, optimal interpolation, and kriging) that build a functional relationship between neighboring and target stations (Simolo et al., 2010). Previous studies have shown that multiple linear regression based on the least absolute deviation criteria (MLAD) performs better than many interpolation methods such as IDW, NR, and optimal interpolation in infilling/reconstruction (Eischeid et al., 2000; Kanda et al., 2018).

3. Quantile mapping (QM) is widely used to correct biases in meteorological data (Maraun, 2013; Cannon et al., 2015) and performs well in estimating missing station data (Simolo et al., 2010; Newman et al., 2015, 2019; Devi et al.,

66   2019). In QM-based estimation, the cumulative distribution functions (CDFs) of observations from neighboring and
67   target stations are derived, and the record at the target station is estimated as the inverse of its CDF using concurrent
68   CDF probability information from neighboring stations. QM can avoid the problem of overestimating wet days in
69   precipitation series and preserve the frequency distribution of time series, which is useful for estimating extreme
70   events (Cannon et al., 2015).

71   4. Machine learning techniques have been successfully applied to infill station record gaps (Dastorani et al., 2010;
72   Wambua et al., 2016). For example, Coulibaly and Evora (2007) estimated missing daily precipitation and
73   temperature in northeastern Canada using six types of artificial neural networks (ANNs). Ustaoglu et al. (2008)
74   estimated daily temperature using three ANN methods in the Geyve and Sakarya basin, Turkey. Gene expression
75   programming was applied in the estimation of missing monthly rainfall data in Malaysia (Che Ghani et al., 2014).
76   Sattari et al. (2017) recommended that a decision-tree algorithm can be used to estimate monthly precipitation due
77   to its simplicity and high accuracy. Serrano-Notivoli et al. (2019) applied the k-nearest neighbours regression to
78   reconstruct minimum temperature (T_{min}) and maximum temperature (T_{max}) observations in Spain to form a gridded
79   dataset.

80   Previous SCDs have been developed using multiple infilling and reconstruction methods. For instance, Eischeid et al.
81   (2000) produced a daily SCD from 1951 to 1991 for the western United States (U.S.), including 2962 precipitation
82   stations and 2034 temperature stations; Vicente-Serrano et al. (2003) produced a daily SCD from 1901 to 2002 for
83   northeast Spain using 3106 precipitation stations; Di Piazza et al. (2011) built a monthly SCD from 1921 to 2004 for
84   Sicily, Italy using 247 precipitation stations; and Woldesenbet et al. (2017) produced a daily SCD of precipitation and
85   temperature from 1980 to 2013 for the Upper Blue Nile Basin using six stations. There is currently no SCD for North
86   America; this means that researchers often must collect station data from different databases, which is time-consuming
87   and may cause inconsistencies between studies based on different methods.

88   Responding to this need, we develop a retrospective 40-year daily SCD for North America (SCDNA) of precipitation,
89   T_{min} and T_{max} from 1979 to 2018. Central America and Caribbean are also covered by SCDNA. The three variables
90   are selected because (1) most stations measure precipitation and temperature, while other variables, such as humidity
91   and wind speed are measured at fewer stations, and (2) precipitation and temperature data are fundamental inputs for
92   hydrological modeling. Station observations are collected from four global and regional databases and undergo strict
93   quality control to eliminate dubious records. Since the performance of infilling and reconstruction methods differs in
94   space and time, the results from 16 strategies are merged to produce a single deterministic estimate. Finally, the
95   SCDNA is compared to four gridded products to demonstrate its performance and areas for improvement. The SCDNA
96   is expected to have a wide variety of applications in North America, and the methodology can be used to produce
97   SCDs in other regions of the world.

2 Datasets

2.1 Meteorological station data

This study uses precipitation, T_{min}, and T_{max} station data from four databases, the Global Historical Climate Network Daily (GHCN-D; https://www.ncdc.noaa.gov/ghcnd-data-access; Menne et al., 2012), the Global Surface Summary of the Day (GSOD; https://catalog.data.gov/dataset/global-surface-summary-of-the-day-gsod), Environment and Climate Change Canada (ECCC; https://climate.weather.gc.ca/historical_data/search_historic_data_e.html), and the Mexico database from Servicio Meteorológico Nacional, under the Comisión Nacional del Agua (Livneh et al., 2015). This study uses daily precipitation totals from each dataset. Only stations with at least 8-year precipitation or T_{min} and T_{max} records between 1979 to 2018 are utilized. The requirement for minimum recording length is different among studies (e.g., Eischeid et al., 2000; Newman et al., 2015). We adopted a relatively short time limitation because (1) 8-year records are sufficient to provide basic support for missing value estimation (Fig. S1), and (2) the open-access dataset and codes enable users to design customized data selection criteria according to their research requirements.

The numbers of stations with at least 8-year records are 33026, 4619, 3634, and 4049 for GHCN-D, GSOD, ECCC, and the Mexico database, respectively (Table 1). Their spatial distributions are shown in Fig. S2. GHCN-D has compiled a large amount of data from many sources including the Mexico database and ECCC. For identical stations from different sources, we keep the one with longer observation history, resulting in the exclusion of ~95% of stations from the Mexico database and adoption of ~91% of stations from ECCC. Stations with more than 30% missing values in the observation period are excluded because they could be seasonal stations or suffer serious instrumentation problems. Stations overlapping in space (same latitude and longitude) and without sufficient metadata for discrimination are merged (see Sect. 3.2). The above screening reduces the available stations from 45328 to 31772 (Table 1), yet more stations are discarded due to quality control procedures (Sect. 3.1). The final SCDNA includes 24615 precipitation, 19604 T_{min}, and 19611 T_{max} stations; note that the numbers of T_{min} and T_{max} stations differ as quality controls can result in excluding the one and reserving the other in some stations.

Most stations are located in the Contiguous United States (CONUS), southern Canada, and Mexico, while few stations are located in high-latitude regions such as the Arctic Archipelago (Fig. 1b and c). The spatial distributions of precipitation and temperature stations are similar, except in eastern CONUS where precipitation stations have a higher density.

Table 1. Numbers of stations with at least 8-year records from 1979 to 2018

Station numbers	GHCN-D	GSOD	ECCC	Mexico	Merge	Total
Original numbers	33026	4619	3634	4049	0	45328
SCDNA input	24765	4331	3100	187	207	31772
SCDNA output: precipitation	19255	2551	2440	170	199	24615
SCDNA output: T_{min}	13394	3631	2219	166	194	19604

SCDNA output: T_{max}	13402	3632	2217	166	194	19611

Notification: "Merge" is derived from stations with overlapped locations from all the other data sources (Sect. 3.1.1).
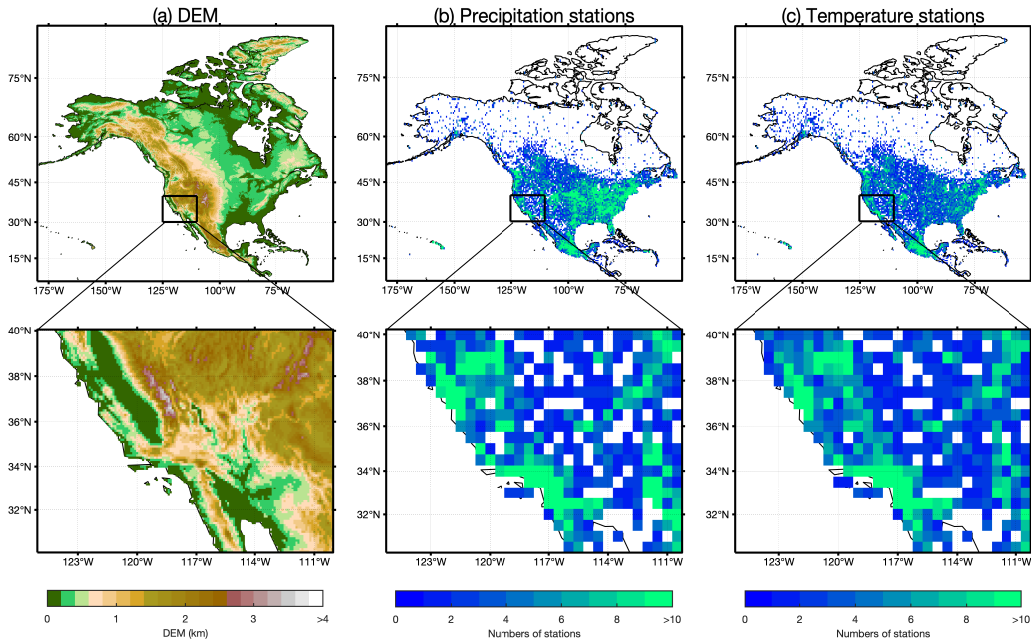
Figure 1. (a) Digital elevation model (DEM; Sect. 2.3) of North America. (b) and (c) are the densities of stations at the 0.5°×0.5° resolution for precipitation and temperature, respectively. T_{min} and T_{max} stations are highly consistent, and thus T_{min} is used to represent temperature in (c). The nested black boxes show examples of DEM and station densities.

In North America, more station observations occur in the U.S. than in Canada and Mexico (Fig. 2). The number of samples in the U.S. increases from 1979 to 2018, and there are more precipitation samples than temperature samples. For Canada, the numbers of precipitation and temperature samples are similar and show a decrease from 1988 to 2018; the sample number in 2018 is only 61.76% of that in 1988. Mexico has more meteorological samples than Canada, yet this number decreases after 1983. The decreasing trend is especially sharp after 2012 which may be due to the delay in data collection or termination of some stations.

Figure 3 shows the fractions of missing values for all stations during the observation period (referred as ratio-1) and during the entire period from 1979 to 2018 (referred as ratio-2). For temperature, ~20% of the stations have more than 20% missing values in the observation period (ratio-1), and ~20% of the stations have more than 70% missing values in the entire period (ratio-2). For precipitation, the fraction of missing values is larger. The fractions show strong spatial variations (Fig. S3). Ratio-2 is smaller for precipitation stations in western U.S. and temperature stations in central U.S., but larger in Canada and Alaska. Most stations in Mexico have higher ratio-1 than other regions in North America, indicating that those stations have notable fractions of missing values during the observation period.

145 In summary, the curves of ratio-1 indicate that a small number of missing values need infilling during the observation
146 period, while the curves of ratio-2 indicate that extensive reconstruction is needed over the entire period.
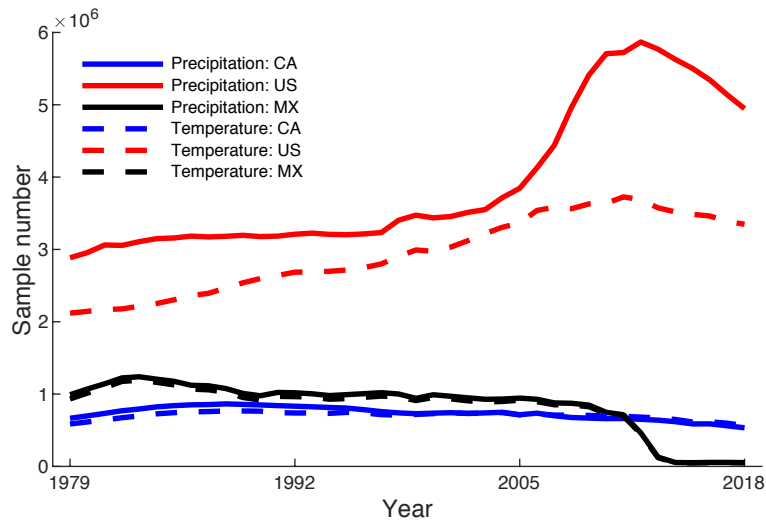
147

148 Figure 2. Sample numbers of stations for each year from 1979 to 2018. CA represents Canada, US represents United
149 States, and MX represents Mexico. T_{max} stations are highly consistent with T_{min} stations, and thus T_{min} is used to
150 represent temperature. The numbers of samples could be a better indicator than the numbers of stations because many
151 stations have notable missing values.

152
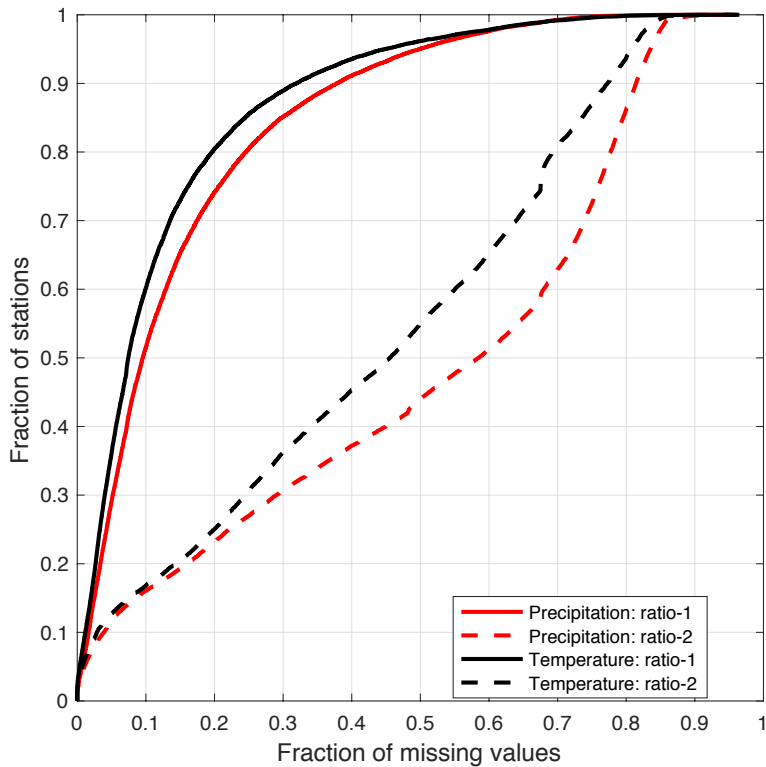
Figure 3. The fraction of missing values for stations with at least 8-year records. Ratio-1 is the degree of missingness during the observation period, and ratio-2 is the degree of missingness during the entire period of interest (1979 to 2018). T_{min} is used to represent temperature because T_{max} show almost overlapped curves with T_{min}.

Many types of precipitation and temperature measurement instruments are used at stations from different sources. For example, the Type-B rain gauge is used by Environment Canada since 1970s for most weather stations (Devine and Mekis, 2008; Wang et al., 2017), while tipping bucket and weighing rain gauges are also used in some stations (Metcalfe et al., 1997). Nipher-shielded snow gauges have been used by some synoptic stations, while ruler measurements are still used by more stations (Mekis and Brown, 2010). Station data in the U.S. are from many organizations or programs with different instrument configurations. For instance, the standard rain gauge is used by the Cooperative Observer Program while Snow Telemetry uses storage-type gauges or tipping buckets. A better understanding of instrument specifications and historical changes is important for climate studies (Pielke Sr et al., 2007; Whitfield, 2014; Ma et al., 2019). A detailed summary of station instruments is provided in the documentation of the dataset (https://doi.org/10.5281/zenodo.3735533).

2.2 Reanalysis products

We use reanalysis precipitation, T_{min} and T_{max} from the fifth generation of European Centre for Medium-Range Weather Forecasts (ECMWF) atmospheric reanalyses of the global climate (ERA5; Copernicus Climate Change Service (C3S), 2017), the Japanese 55-year Reanalysis (JRA-55; Kobayashi et al., 2015), and the Modern-Era Retrospective analysis for Research and Applications, Version 2 (MERRA-2; Gelaro et al., 2017) (see Table 2). The three products are chosen because they are representative products from different international organizations and they or their predecessor (ERA-Interim, JRA-25, and MERRA) have are been widely used by researchers. The ERA5 and JRA-55 do not provide daily outputs, thus, daily precipitation is accumulated from sub-daily estimates while daily T_{min} and T_{max} are estimated by the sub-daily minimum and maximum temperature values. Gridded reanalysis precipitation is linearly interpolated to match point-scale station data, and T_{min} and T_{max} are downscaled using temperature lapse rate (TLR; see Sect. 3.1).

Table 2. Information on the three reanalysis products.

Products	Spatial resolution	Temporal resolution	Period	Agency
ERA5	0.25°×0.25°	1 h	1979-present	European Centre for Medium-Range Weather Forecasts
JRA-55	~55 km	3 h	1958-present	Japan Meteorological Agency
MERRA-2*	0.5°×0.625°	daily	1980-present	NASA's Global Modeling and Assimilation Office

* MERRA-2 provides outputs in temporal resolutions from 1 h to 1 month; here we use daily values.

2.3 Auxiliary data

The Multi-Error-Removed Improved-Terrain digital elevation model (MERIT DEM) at a 3 sec (~90 m at the equator) resolution (Yamazaki et al., 2017) is used in this study. To enable temperature downscaling, the high-resolution DEM is spatially averaged to the original resolutions of ERA5, MERRA-2, and JRA-55 (Table 2). The MERIT DEM may be slightly different than the DEM data used in the three reanalysis products, and this will have a limited impact on missing data estimation (Sect. 3.3.2).

The Multi-Source Weighted-Ensemble Precipitation (MSWEP) V2.2 dataset (Beck et al., 2017, 2019) is utilized for the comparison with the SCDNA developed by this study. MSWEP merges data from ground observations, satellite products, and reanalysis models, and performs better than all products used for merging (Beck et al., 2019). The comparison can show whether the SCDNA is a better choice than MSWEP to fill gaps in station precipitation observations.

3 Methodology

The methodology to produce the SCDNA includes three primary steps (Fig. 4): (1) preparing a unified precipitation and temperature database from multiple sources (Sect. 2.1 and 3.1); (2) downscaling reanalysis estimates (Sect. 2.2 and 3.2) that are used in QM- and machine learning-based data estimation (Sect. 3.3) and comparison with the SCDNA (Sect. 4.5); and (3) producing the SCDNA from 1979 to 2018 based on 16 strategies (Sect. 3.3). The following sub-sections summarize the work in each step of the methodology (Sect. 3.1, 3.2, and 3.3) as well as the approach used to evaluate the performance of the method (Sect. 3.4).

197
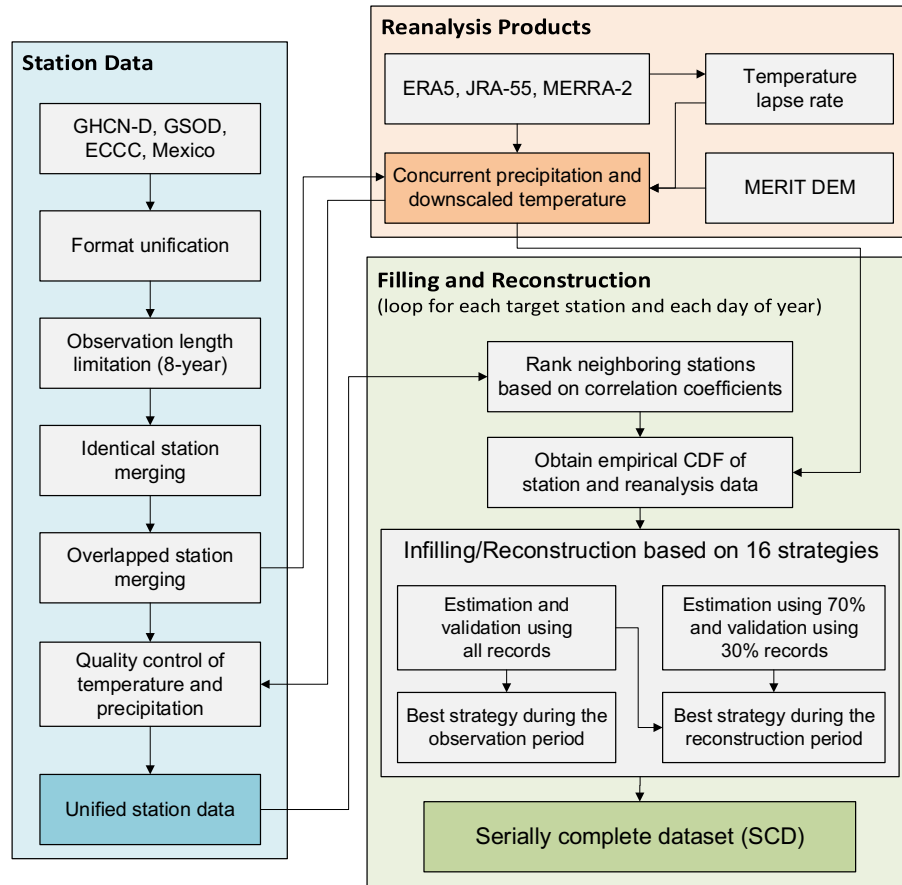
Figure 4. Flowchart of the production of the SCDNA, including station data preparation, reanalysis product processing, and missing data infilling and reconstruction.

In this study, infilling refers to the estimation of missing values during the observation period, while reconstruction refers to estimating values outside of the observation period when no station record is available (Fig. 5). Station records that fail quality control are treated as missing values.

3.1 Prepare a unified precipitation and temperature database

3.1.1 Merging of stations based on location

Stations are merged if their latitude and longitude match other stations. The problem of overlapped locations is caused by identification alteration of one station for different periods, recording/rounding bias of station location information, inconsistent naming rules of different sources, and other factors. Although it is possible that multiple stations are deployed in the same location for experimental aims, location merging is done to preserve internal consistencies as inconsistent records at the same location are self-contradictory.

The method for location merging includes several steps. First, overlapping stations are extracted and grouped. Stations within the same group that have non-overlapping recording periods are simply merged into one time series. Otherwise,

212   the Spearman's rank CC (SCC) between precipitation series from all station pairs in the group is calculated. For SCC

213   < 0.7, the station group is discarded due to large discrepancies; for 0.7 < SCC < 0.9 the discrepancy is considered as

214   tolerable and the station with the longest record is kept; for SCC > 0.9 stations are considered as highly correlated and

215   their data are merged into one time series, while for overlapping periods the station with the longest record is used.

216   Overall, 1240 stations are involved in location merging, stratified in 586 station groups. Around 10% of the groups

217   contain more than two stations and the largest group contains five stations. After location merging, only 207 groups

218   are kept and merged into unified times series (Table 1). Despite the steps taken above, the merged series could contain

219   inhomogeneities due to the combination of records from multiple stations.

220   *3.1.2 Quality control*

221   To ensure station observations undergo strict and comprehensive quality control, we adopted the methods used to

222   produce previous station-based datasets. For T_{min} and T_{max}, we followed the method designed by Durre et al. (2010)

223   which is adopted by GHCN-D (Menne et al., 2012). The procedures include five types of checks: integrity checks,

224   outlier checks, internal and temporal consistency checks, spatial consistency checks, and extreme megaconsistency

225   checks. A few of the procedures in Durre et al. (2010) require other variables such as snowfall, and thus are not

226   adopted in this study. In addition, the quality flags in this study are partly different with those of GHCN-D because of

227   the different sources, numbers and temporal periods of stations.

228   For precipitation, quality control procedures consist of three parts. The first part is similar with that for temperature.

229   The second part (four types of checks) follows procedures designed by Hamada et al. (2011) which are adopted by

230   the Asian Precipitation-Highly-Resolved Observational Data Integration Towards Evaluation (APHRODITE; Yatagai

231   et al., 2012). The third part (two types of checks) adopts strategies by Beck et al. (2019) used in the production of

232   MSWEP. Note that although Durre et al. (2010) and Hamada et al. (2011) share some common traits for precipitation,

233   both of them are adopted to ensure quality control reliability.

234   The details of quality checks are in Appendix B.

235   **3.2 Downscale reanalysis data**

236   The reanalysis temperature estimates are downscaled to match point-scale station observations using temperature lapse

237   rate (TLR) according to

$$T_s = T_R + \text{TLR} \times \Delta h \tag{1}$$

238   where T_R is 2-m reanalysis air temperature, T_s is downscaled temperature, Δh is the height difference between station

239   elevation and reanalysis grid elevation. TLR shows notable spatiotemporal variations (Minder et al., 2010) and

240   estimating TLR based on ground observations over a large domain is difficult due to the sparsity of stations. Yet recent

241   studies show that reanalysis outputs offer an alternative in estimating gridded TLR (e.g., Gao et al., 2012). The gradient

242   of air temperature at different pressure levels above the ground can be used to approximate near-surface TLR (Gao et

al., 2012, 2018; Gruber, 2012). Tang et al. (2018) compared eight temperature downscaling methods in CONUS and found that methods based on reanalysis-derived TLR can achieve higher accuracy compared to fixed TLR (e.g., -6.5°C/km) or statistical interpolation downscaling methods. Hence, this study uses the linear regression slope between MERRA-2 air temperature and geopotential heights from 300 hPa to 1000 hPa pressure levels to represent TLR for each month at the resolution of 0.5°×0.625° (Table 2). MERRA-2 is used because it directly provides monthly data and masks temperature data if the pressure level is below land surface. The choice of pressure levels needs further investigation because relationships between vertical and near-surface temperature vary with regions. Complicated TLR phenomena such as inverse lapse rate are not considered for simplicity. The climatological mean of TLR (Fig. S4) decreases from -4.8°C/km in the northeast continent (i.e., Canadian Arctic Archipelago) to -7.2°C/km in the southwest continent (i.e., Rocky Mountains in CONUS). The smaller TLR magnitude in high latitudes is consistent with previous studies (e.g., Gardner et al., 2009; Marshall et al., 2007).

3.3 Produce the serially complete dataset

To produce the high-quality SCDNA for North America, we use 16 strategies: four based on quantile mapping with neighboring stations (QMN; e.g., Longman et al., 2019; Newman et al., 2015, 2019), four on quantile mapping with concurrent reanalysis estimates (QMR), four using spatial interpolation methods (INT; e.g., Eischeid et al., 2000; Kanda et al., 2018; Woldesenbet et al., 2017), two using machine learning methods (MAL; e.g., Dastorani et al., 2010; Wambua et al., 2016), and two multi-strategy merging methods (MRG). Merging multiple infilling/reconstruction methods can provide better estimation than individual methods, as shown by previous data merging and gap infilling studies (e.g., Eischeid et al., 2000; Beck et al., 2017, 2019; Ma et al., 2018).

We generate estimates for every station and every day from 1979 to 2018 (Fig. 5). The estimates from these 16 strategies and the SCDNA are evaluated using station observations, and the performance of the SCDNA is compared to four benchmark gridded products. Then, the estimates of the SCDNA are corrected for further accuracy improvement. Finally, estimates are replaced by station observations when observations exist and pass quality control checks. The variance and spatial correlation analyses are performed to compare the statistical properties of station observations and estimates (see Sect. 4).

268
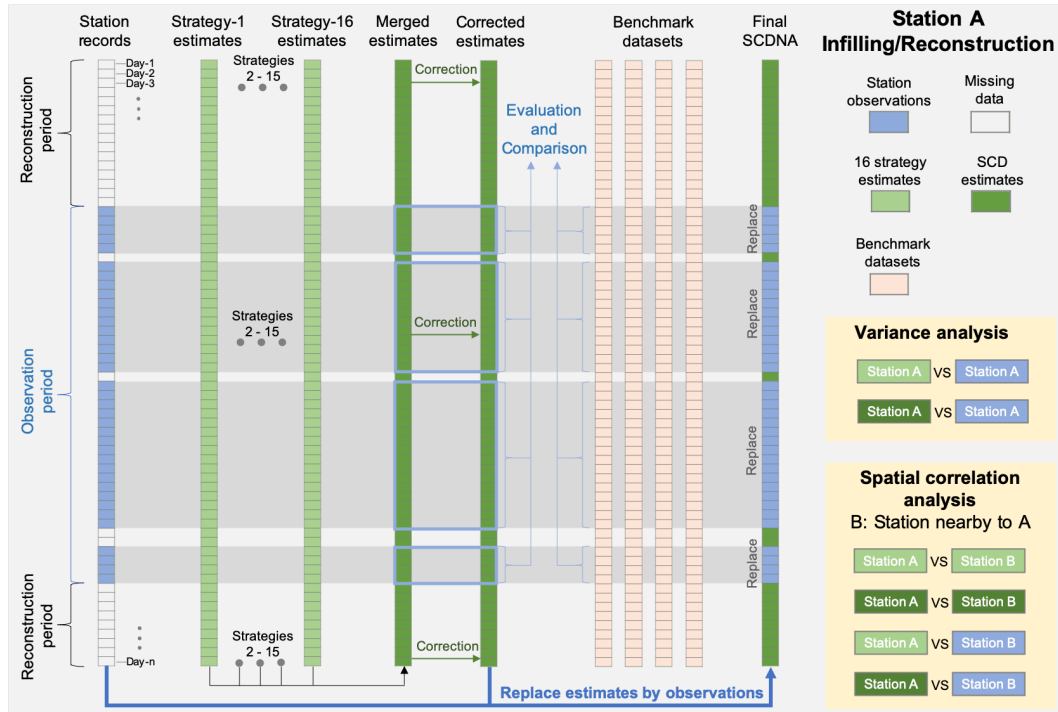
Figure 5. Diagram of the infilling and reconstruction for a specific station (referred to as A). The entire period from 1979 to 2018 is divided into the observation period and the reconstruction period. The data flows of variance and spatial correlation analyses are shown in the nested yellow boxes. Station B is a nearby station of A.

Only stations with at least 3000 valid values are included in the infilling and reconstruction effort. The nine steps (termed Step-1 to Step-9) of SCDNA production are described as below. Unless otherwise stated, the steps are implemented for each target station (s), each variable (precipitation, T_{min}, and T_{max}), and each day of the year (DOY, i.e., 1-366).

3.3.1 Data extraction

Step-1: Spatiotemporally concurrent reanalysis estimates (ERA5, JRA-55, and MERRA-2) are extracted, including precipitation, T_{min}, T_{max}, and TLR. Precipitation is linearly interpolated from gridded reanalysis estimates, and temperature is downscaled (i.e., corrected for the elevation difference between the reanalysis grid cell and the station elevation) based on TLR (Sect. 3.1).

Step-2: Neighboring stations (at least one and at most 30) with at least 8-year overlapped period with station s are found within the searching radius of 200 km. These stations are ranked from closest to farthest according to their CC with the target station. SCC is used for precipitation, and Pearson CC (PCC) is used for T_{min} and T_{max}. CC is calculated using data within a 31-day window centered around the current DOY from all years.

Step-3: The empirical CDFs of s, neighboring stations, and reanalysis estimates are obtained using data within the same 31-day window.

287   *3.3.2 Infilling and reconstruction*

288   **Step-4**: For each day (*d*) corresponding to the DOY, the estimated data are acquired based on 16 strategies which are
289   divided into five groups.

290   *Group 1*: **Quantile Mapping with Neighboring stations (QMN)**

291   •   **QMN-1**: For all neighboring stations with valid records, the station with the highest CC in Step-2 is selected.
292   The estimated data for *s* and *d* is obtained using Eq. (2).

$$X_s = F_s^{-1}(F_i(X_i)) \tag{2}$$

293   where X_i is precipitation or temperature for *d* from the selected neighboring station *i*, F_i is the empirical CDF of
294   *i* corresponding to the DOY, F_s^{-1} is the inverse CDF of *s* corresponding to the DOY, and X_s is the estimated data.

295   •   **QMN-2**: For all neighboring stations with observations, estimated values are obtained using Eq. (2) which are
296   merged based on Eq. (3).

$$X_s = \frac{\sum_i^n W_i F_s^{-1}(F_i(X_i))}{\sum_i^n W_i} \tag{3}$$

$$W_i = CC_i^2 \tag{4}$$

297   where *n* is the number of neighboring stations, $F_s^{-1}(F_i(X_i))$ is the QM-based estimate from *i*, and W_i is the weight
298   calculated using Eq. (4). CC_i is CC (SCC or PCC) between data from *s* and *i* corresponding to the DOY. W_i is
299   assigned zero if CC_i is negative.

300   •   **QMN-3**: Similar to QMN-2, but the weight is calculated according to the distance (D_i) between *s* and *i* based on
301   Eq. (5). Although the exponent of distance (*k*) varies in different studies, -2 is the most common choice
302   (Teegavarapu and Chandramouli, 2005).

$$W_i = D_i^k \tag{5}$$

303   •   **QMN-4**: The median of QMN-1 to QMN-3 is used as the estimated data. The strategy of using median values is
304   the same with Eischeid et al (2000), which could be closer to actual observations than QMN-1 to 3.

305   *Group 2*: **Quantile Mapping with Reanalysis products (QMR)**

306   Reanalysis products provide useful information for SCDNA production as (1) remote regions may not have enough
307   neighboring stations, and (2) neighboring stations also have missing values which could result in gaps of estimates at
308   the target station.

309   •   **QMR-1 to QMR-3**: Similar to QMN-1, but the neighboring station is replaced by concurrent ERA5, JRA-55,
310   and MERRA-2 estimates, respectively.

311   •   **QMR-4**: The median of QMR-1 to 3 is used as the estimated data.

312   *Group 3*: **Interpolation (INT)**

313 The three interpolation methods used in this study are MLAD (referred as INT-1), NR (referred as INT-2), and inverse
314 distance weighting (IDW, referred as INT-3). They are described below. Following Eischeid et al. (2000), neighboring
315 stations with CC lower than 0.35 are excluded. The remaining stations are ranked from high CC to low CC. A
316 maximum of four neighboring stations are used in the interpolation. For T_{min} and T_{max}, direct interpolation from
317 neighboring stations to s could be biased due to the elevation differences between stations. Temperature data from
318 neighboring stations are downscaled to the elevation of s based on Eq. (1).

319   •   **INT-1**: MLAD minimizes the sum of absolute errors. It is more robust than regression based on least squares
320   because while least square estimation is effective when the errors are normally distributed and independent,
321   environmental variables, especially precipitation, often violate the assumption of normality (Eischeid et al.,
322   2000). MLAD has been well documented with better performance in gap infilling than other interpolation
323   methods (Eischeid et al., 1995, 2000; Kanda et al., 2018; Young, 1992). The formula is shown in Eq. (6).

$$X_s = c_0 + \sum_{i}^{n} c_i X_i \tag{6}$$

324   where c_i ($i = 0, 1, …, n$) is regression coefficients estimated using data within a 31-day window for each DOY.
325   Different d corresponding to the same DOY could have different combinations of neighboring stations due to the
326   limitation of observation availability. MLAD is performed for each combination to ensure that effective estimates
327   are available for all days.

328   •   **INT-2:** NR is an interpolation method proposed by Paulhus and Kohler (1952) and modified by Young (1992).
329   The modified version is adopted in this study, which combines information from neighboring stations by
330   replacing $F_s^{-1}(F_i(X_i))$ with X_i in Eq. (3). The weight is calculated using Eq. (7).

$$W_i = CC_i^2 \frac{N_i - 2}{1 - CC_i^2} \tag{7}$$

331   where N_i is the number of samples used to calculate CC_i between s and i. SCC is used for precipitation and PCC
332   is used for temperature.

333   •   **INT-3**: IDW is one of the most common interpolation methods. It is implemented similar to NR, where the
334   inverse squared distance, as shown in Eq. (5), is used as the weight.

335   •   **INT-4**: The median of INT1, INT2 and INT3 is used as the estimated data.

336 *Group 4*: **Machine Learning (MAL)**

337 The two MAL methods used in this study are ANN (referred as MAL-1) and random forest (RF, referred as MAL-2;
338 Breiman, 2001). Unlike QMN, QMR and INT that are carried out for each DOY, MAL uses complete observation
339 records of *s* to ensure that ANN and RF are trained with enough values. MAL models are trained using the first 70%
340 observations and tested using the remaining 30% observations. The MAL models' validation based on the 30%
341 observations can indicate their performance in the reconstruction period.

342 The input data are from neighboring stations and concurrent reanalysis estimates. For each *s*, neighboring stations are
343 determined in a way similar with Step-2, but CC is calculated using data in the entire observation period. Neighboring
344 stations with CC lower than all reanalysis products (ERA5, JRA-55, and MERRA-2) are excluded. The remaining
345 neighboring stations and three reanalysis products form a complete repository of input features. Then, for each day
346 that *s* has no observation, the input features are extracted from the repository in three steps: (1) neighboring stations
347 without observations for the day are excluded, (2) the remaining neighboring stations and reanalysis products are
348 ranked according to their CC with *s*, and (3) at most five stations/reanalysis products with the highest CC are selected.
349 In this way, *s* will have multiple combinations of input features to ensure that all days with missing values have
350 estimates. All combinations are used to train and test the ANN and RF models, resulting in multiple estimated series
351 for *s*. The final estimates of *s* are generated in three steps: (1) the Kling-Gupta Efficiency (KGE'; Kling et al., 2012)
352 of all estimated series is calculated using all observations of *s*, and ranked from high to low KGE' (see Sect. 3.4 for
353 definition of KGE'); (2) the series with higher KGE' is used to constitute the estimates of *s* in sequence; and (3) the
354 second step is repeated until there are no missing values for *s*. This approach ensures that "best" and complete estimates
355 are provided for *s*.

356   •   **MAL-1**: A four-layer ANN is used. The input layer has a maximum of five nodes (depending on the number of
357   input features), the two hidden layers both have 20 nodes, and the output layer has one node for generating
358   precipitation or temperature estimates. The transfer functions are hyperbolic tangent sigmoid for hidden layers
359   and linear for the output layer. The training function is resilient backpropagation. The model is trained using the
360   first 50% data, validated using the subsequent 20% data, and tested using the final 30% data.

361   •   **MAL-2**: A RF model with 50 trees is built with 70% training data and 30% testing data. The minimum number
362   of samples per tree leaf is 5. The input nodes depend on the number of input features like MAL-1.

363 *Group 5*: **Multi-Strategy Merging (MRG)**

364   •   **MRG-1**: KGE' is used to rank the performance of the 11 strategies (QMN-1 to 3, QMR-1 to 3, INT-1 to 3,
365   and MAL-1 to 2) as CC cannot reflect the magnitude difference (e.g., bias) between target and reference

366   series. The first three cases of the 11 strategies are merged using squared KGE' as the weight. The individual
367   weight is assigned zero if KGE' is negative.

368   - **MRG-2**: The median of the three selected strategies in MRG-1 is used as the estimated data.

369   *3.3.3 Generating serially complete records*

370   **Step-5**: In this step, Step-3 and -4 are repeated based on 70% data of s in the observation period. Then, the KGE' of
371   estimates from all strategies are calculated using the remaining 30% observations. MAL-1 and 2 are not repeated
372   because they are trained on 70% observations. Although the evaluation samples are different among stations, the
373   results are reliable and stable as shown in the results section. This step is implemented because QMN-1 to 4, QMR-1
374   to 4, and INT-1 in Step-4 use all data of s in the observation period to select stations, estimate empirical CDFs and
375   carry out regression. This potential overfitting problem could lead to better performance of these strategies in the
376   observation period but worse performance in the reconstruction period. KGE' calculated in Step-4 can represent the
377   accuracy of estimates in the observation period, while KGE' calculated in Step-5 can represent the accuracy of
378   estimates in the reconstruction period.

379   **Step-6**: In the observation period, the strategy with the highest KGE' in Step-4 is selected to contribute the
380   extension/reconstruction to the SCDNA. In the reconstruction period, first, the strategy with the highest KGE' in Step-
381   5 is determined; then, the estimates from the corresponding strategy in Step-4 are used to constitute the SCDNA
382   because the empirical CDF and regression based on all observations in Step-4 could be more representative than the
383   70% observations in Step-5.

384   **Step-7**: Estimates in Step-6 are corrected for certain climatological biases using station data in the observation period.
385   Precipitation estimates are often subjected to wet-day bias. Two methods are implemented to address this problem.
386   First, QM is performed based on the CDF of s in Step-3. However, QM may reduce the accuracy of estimated
387   precipitation in some cases, for which the method used in Beck et al. (2019) is adopted. This method subtracts a tiny
388   value (0.01 mm) from the original precipitation series and rescales the series to restore the original mean value. This
389   operation is repeated until the estimated series show an equal number of wet days (>0.5 mm d^{-1}) with observations of
390   s. In addition to wet-day bias correction, mean-value correction is implemented. The ratio between the mean values
391   of precipitation estimates and observations is calculated in the observation period, which is used to rescale estimated
392   series in both observation and reconstruction periods. For T_{min} and T_{max}, QM correction and mean-value correction are
393   also implemented.

394   **Step-8**: The accuracy of the SCDNA is evaluated and compared to benchmark datasets based on actual observations
395   (Fig. 5). Then, the estimates are replaced by observations whenever possible to generate the final SCDNA. Very
396   occasionally, estimated T_{min} could be larger than estimated T_{max}, for which T_{max} is replaced by the maximum T_{max}, and
397   T_{min} is replaced by the minimum T_{min} of the estimates from the 16 strategies.

398   **Step-9**: The serially complete data of SCDNA is quality controlled again using methods introduced Sect. 3.1.2 to
399   exclude stations with unreliable estimates.

400   **3.4 Evaluate the precipitation and temperature estimates**

401   KGE', which is proposed by Gupta et al. (2009) and modified by Kling et al. (2012), is used to support the merging
402   of different strategies (Sect. 3.3) and the evaluation of the estimated precipitation and temperature.

$$\begin{cases} \mathrm{KGE}' = 1 - \sqrt{(r-1)^2 + (\beta-1)^2 + (\gamma-1)^2} \\ \beta = \dfrac{\mu_s}{\mu_0} \\ \gamma = \dfrac{CV_s}{CV_0} = \dfrac{\sigma_s/\mu_s}{\sigma_o/\mu_o} \end{cases} \tag{8}$$

403   where r is the PCC, β is the bias ratio, and γ is the variability ratio; μ is the mean value, and σ is the standard
404   deviation. The subscripts s and o represent estimated and reference time series, respectively. KGE' ranges from
405   negative infinity to one. If two series exactly match, the KGE' is one. A β or γ value smaller/larger than one indicates
406   that the mean value or variability of observations is underestimated/overestimated.

407   In Sect. 4, the evaluation during the observation period is based on the complete station observations (i.e., Step-4 in
408   Sect. 3.3.2), while the evaluation during the reconstruction period is realized using 30% independent station
409   observations (i.e., Step-5 in Sect. 3.3.3). Unless otherwise stated, SCDNA estimates in Sect. 4 are after correction
410   (Step-7 in Sect. 3.3.3). In Sect. 4.5, SCDNA estimates are compared with gridded products (ERA5, JRA-55, MERRA-
411   2, and MSWEP). In addition to the three SCDNA variables (precipitation, T_{min}, and T_{max}), mean temperature (T_{mean},
412   the mean of T_{min} and T_{max}) and daily temperature range (T_{range}, the difference between T_{max} and T_{min}) are also included.
413   The involvement of T_{range} can contribute to more objective comparison between SCDNA and reanalysis products
414   because the TLR-based downscaling of reanalysis temperature contains uncertainties, which could affect the
415   evaluation of T_{min}, T_{max}, and T_{mean}. Although there exist differences between TLR of T_{min} and T_{max}, T_{range} can reduce
416   the effect of scale-mismatch between gridded reanalysis temperature and point station temperature on evaluation
417   results.

418   **4 Results**

419   **4.1 Comparison of infilling and reconstruction strategies**

420   The value of a given infilling/reconstruction strategy can be quantified by the extent that a strategy is selected for use
421   in the final SCDNA dataset. In this sense, the contribution ratios define the proportion of estimates that come from a
422   specific strategy. Fig. 6 shows that the contribution ratios of QMN, QMR, and INT to missing value estimation are
423   generally smaller than 20% in North America. Please note that QMN refers to all strategies within this group unless
424   the strategy number is specified right after QMN. This also applies to other groups. QMR shows the smallest
425   contribution ratios for almost all stations among the five groups. Compared with other regions in North America,

426   contribution ratios of QMR are higher for precipitation stations in western U.S. and temperature stations in Mexico.

427   INT shows lower contribution ratios in the Rocky Mountains compared with the western U.S., indicating statistical

428   interpolation without considering topographic effect is subjected to substantial uncertainties in complex terrain. MAL

429   shows notably higher contribution ratios than QMN, QMR, and INT, particularly for T_{min} and T_{max}. The ratios of MAL

430   are higher than 20% for ~30% precipitation stations, ~65% T_{min} stations, and ~68% T_{max} stations. MRG has the highest

431   contribution ratios throughout North America. The average contribution ratios of MRG are 59.88%, 41.59%, and

432   40.56% for precipitation, T_{min}, and T_{max}, respectively. For precipitation, MRG is particularly effective in high-latitude

433   regions (northern Canada and Alaska), western U.S. and Mexico.
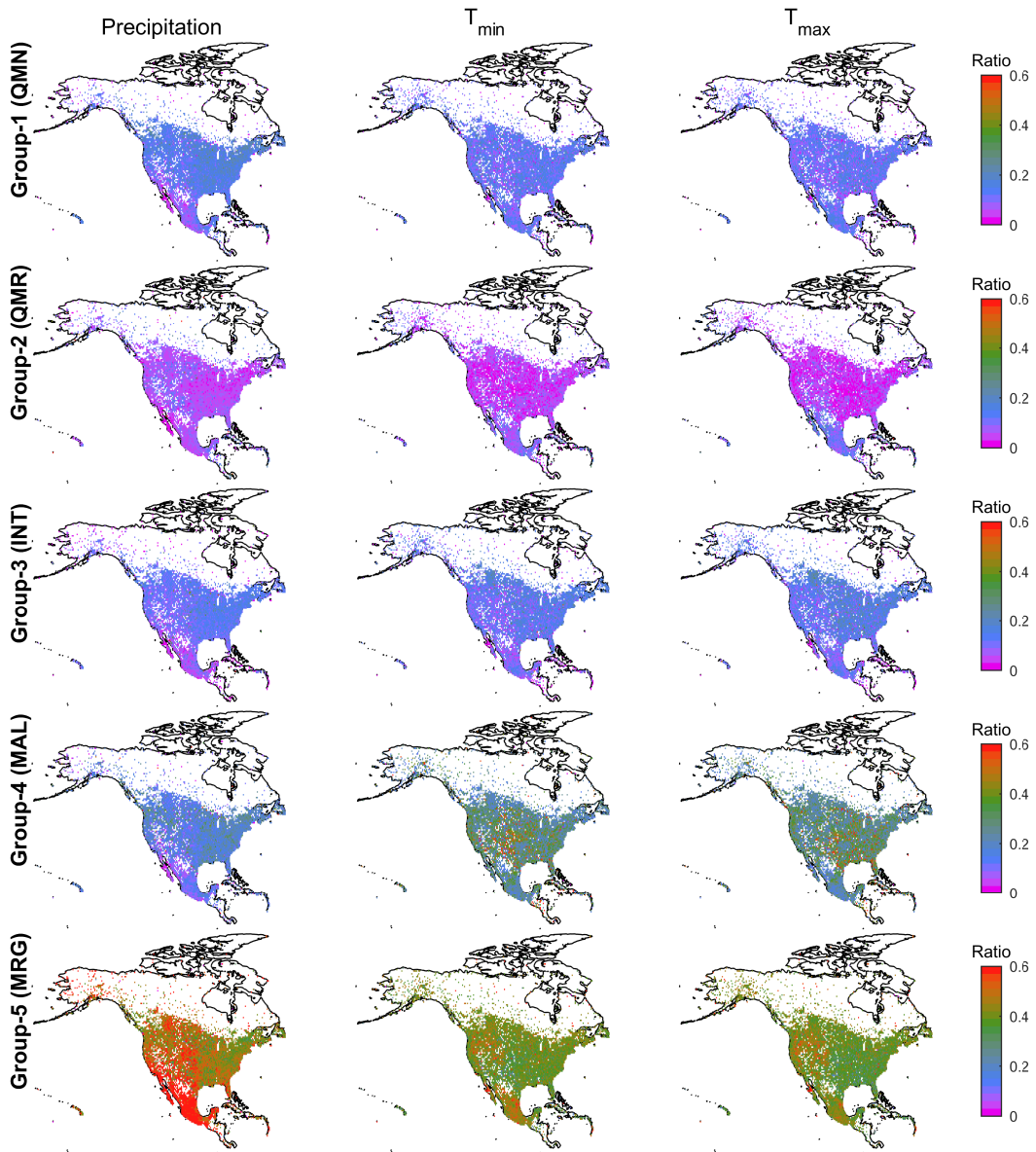
434

435 Figure 6. The contribution ratios of estimates from five infilling/reconstruction groups to the missing values of all
436 stations from 1979 to 2018. The three columns from left to right represent precipitation, T_{min}, and T_{max}, respectively.
437 The five rows from top to bottom represent Group-1 (QMN), Group-2 (QMR), Group-3 (INT), Group-4 (MAL), and
438 Group-5 (MRG), respectively. The maps are at the resolution of 0.5°. The ratio for each grid cell is the mean value of
439 all stations within this grid cell.

440 Figure 7 shows the KGE' and contribution ratios of 16 strategies. The KGE' of estimated precipitation is lower than
441 that of estimated T_{min} and T_{max} due to the stronger spatial and temporal homogeneity of temperature (Fig. 7). The
442 median KGE' values of T_{min} and T_{max} are generally above 0.9, and the accuracy of estimated T_{max} is higher than that
443 of T_{min}. The KGE' during the reconstruction period is smaller than that during the observation period, which is
444 particularly obvious for QMN, QMR, and INT-1 compared with other strategies, because QMN and QMR transfer
445 CDF during the observation period to other periods, and INT-1 transfers regression relationship during the observation
446 period to other periods. MAL suffers a slight degradation in the reconstruction period, and the better performance of
447 MAL-2 than MAL-1 shows that RF could be a better choice than ANN in estimating missing data. For MRG, the
448 differences of KGE' between the two periods are relatively small. For example, the median KGE' values of MRG-1
449 for T_{max} are 0.99 and 0.98 for observation and reconstruction periods, respectively. MRG also shows higher KGE' and
450 a narrower quantile ranges than other strategies, particularly for precipitation, benefiting from merging estimates from
451 multiple strategies

452 Regarding contribution ratios (Fig. 7), strategies with higher KGE' often have larger contributions to the estimated
453 series. However, this is not always true because the selection of strategies is performed for each DOY. Note that the
454 contribution ratios of MAL-2 are even higher than MRG-1 during the observation period for T_{min} and T_{max}, although
455 MRG-1 achieves higher KGE' than MAL-2 for most stations. This is because MAL-2 could be the best choice for
456 more DOY than MRG-1 even though MRG-1 may achieve the best overall performance. An example using T_{min} data
457 from one station is shown in Fig. S5.

458 In the reconstruction period when observations are absent, the contribution ratios of MAL-2 decrease drastically
459 compared with the observation period, contributing to the increased ratios of other strategies (particularly MRG-1).
460 Although QMR shows the lowest contribution ratios, reanalysis products have implicit contributions to other strategies
461 (e.g., MAL and MRG). Overall, MRG-1 shows much higher contribution ratios than all the other strategies (including
462 MRG-2) during the reconstruction periods, indicating that it is the most important strategy in missing value estimation.
463 Hence, combining information from multiple strategies is more reliable, and KGE'-based merging is more effective
464 than the median-value-based estimation.

465

466
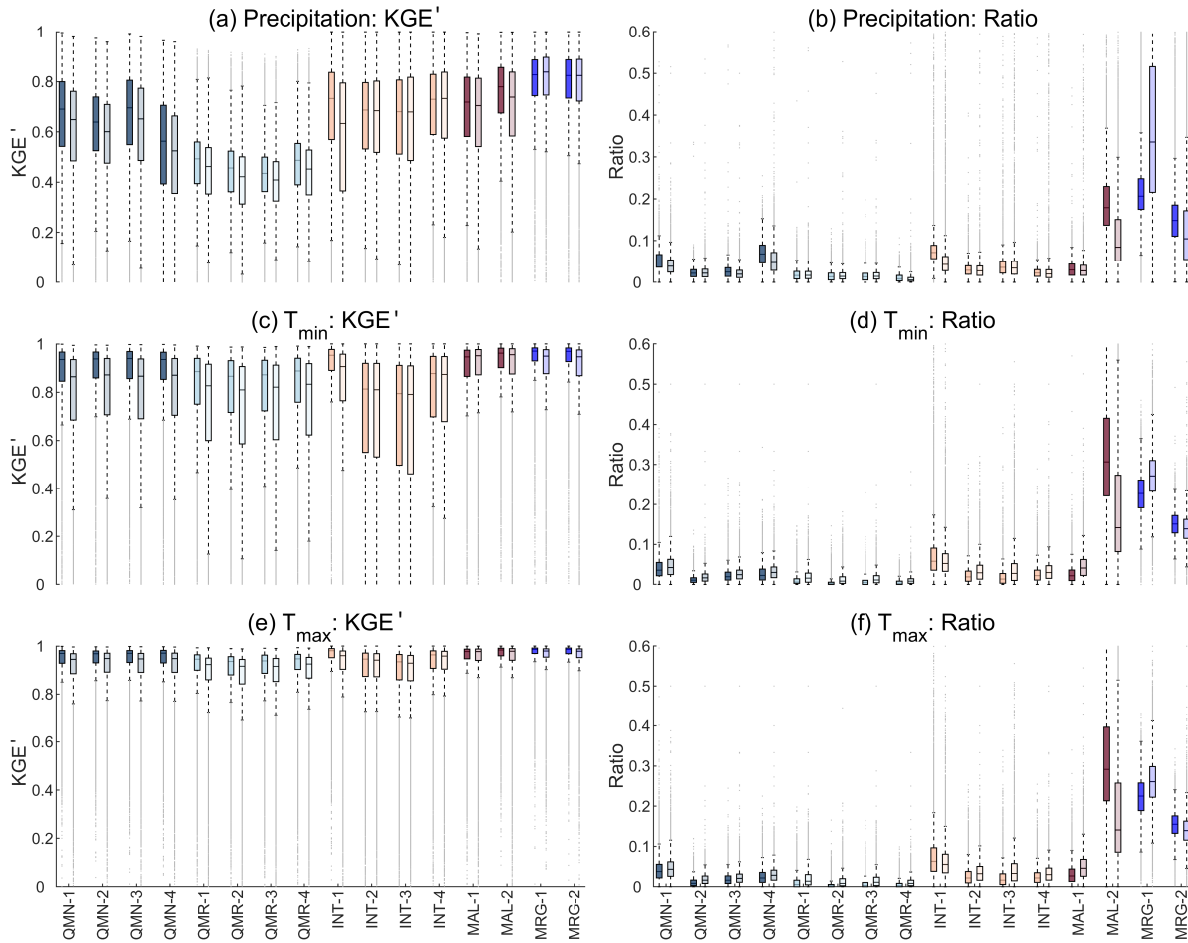
Figure 7. Boxplots of (a, c, and e) the KGE' and (b, d, and f) the contribution ratio of 16 strategies for all stations.
Each strategy corresponds to two boxes in each sub-figure; the left one with darker color represents the observation
period, and the right one with lighter color represents the reconstruction period. The line within the box is the median.
The upper and lower edges of the box represent the 25th and 75th percentiles, respectively. Values more than 1.5
times the interquartile range away from the upper or lower edges are outliers (dots).

4.2 Impact of reconstruction on spatial correlation and series variance

All infilling/reconstruction strategies except QMR rely on information from neighboring stations; this could affect the
spatial correlation structure and the variance of SCDNA series. Space-time correlations and other properties (e.g.,
intermittency of precipitation) are important considerations because they can influence the performance of follow-on
applications that use the SCDNA as input. Theoretically, QMN strategies could significantly inflate spatial correlation
but retain variance of station observations. The spatial correlation inflation in INT strategies could be lower but the
variance would be underestimated due to smoothing. QMR-1 is used as an example to demonstrate the effect of QM
on spatial correlation and series variance (Fig. S6), because QMN uses different station combinations for every DOY
which would mask the effect of QM on final estimates. If the ERA5 used by QMR-1 is replaced by station observations,
the results should be generally consistent. According to Fig. S6, the spatial correlation is substantially inflated by

482   QMR-1, particularly for T_{min} and T_{max}, while the standard deviation of QMR-1 estimates is very close to that of

483   observations. This supports the design of estimating missing data using neighboring stations for each DOY as

484   otherwise, the inflation of CC could be very substantial for the entire period.

485   The spatial correlation based on station observations (Fig. 8a, d, and g) shows obvious seasonal variations, with CC

486   lower in the warm season and higher in the cold season. The seasonality of CC for T_{max} is weaker compared with that

487   for precipitation and T_{min}. The SCDNA estimates capture the seasonal patterns but underestimates the variation (Fig.

488   8b, e, and h) because the inflation of spatial CC is larger in the warm season than cold season (Fig. 8c, f, and i).

489   Moreover, the inflation is larger for neighboring stations with lower correlation with the target station. We tested

490   selecting neighboring stations according to their distance from the target station, and similar results were acquired.

491   For precipitation, the median CC differences of all stations are close to 0.1 in the cold season and range between 0.1

492   and 0.15 in the warm season. For T_{min}, the median CC differences are generally between 0.05 and 0.15. The CC

493   differences of T_{max} are relatively homogeneous for different seasons and generally fluctuate between 0.05 and 0.1. The

494   inflation of CC is because (1) the estimates from the 10 neighboring stations and the target station are generally derived

495   using highly overlapped information (Sect. 3.3.1), and (2) estimation is realized for each DOY for all strategies except

496   MAL, meaning that calculating CC for each DOY show the inflation to the largest extent.

497   The final SCDNA replaces estimates by observations, which can largely relieve the inflation of spatial correlation

498   (Fig. S7), depending on the degree to which observations are present in the record. For T_{min} and T_{max}, CC is very close

499   to that based on observations; for precipitation, correlation in wintertime is even lower than that based on observations.
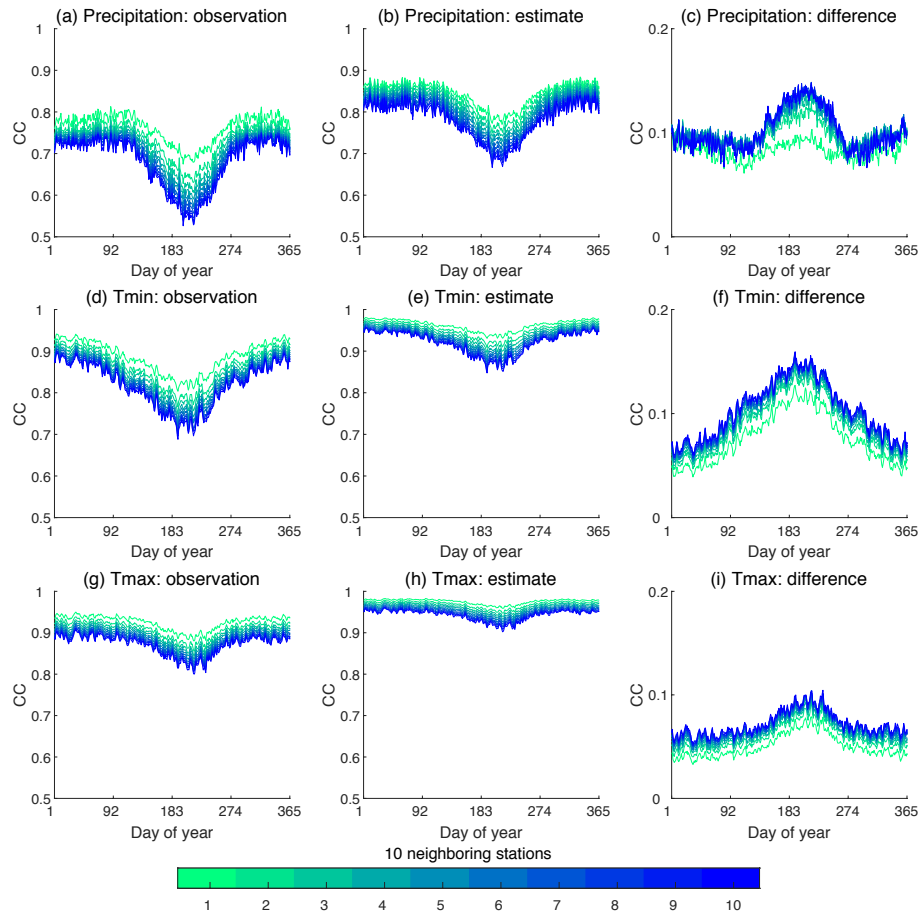
Figure 8. CC between target and neighboring stations for all DOY using station observations (the first column), SCDNA estimates (second column), and differences between SCDNA- and observation-based CC (the third column). CC is calculated in the observation period. For each target station, 10 neighboring stations are selected according to the correlation between time series from target and neighboring stations. Smaller numbers represent higher correlation. For example, station 1 represents the neighbor with the highest CC with the target station. Each curve represents the median CC of all stations.

Figures 9 and 10 show CC between estimates at the target station and observations at the neighboring station. For precipitation, most strategies exhibit similar spatial correlation structure with observations for most stations. QMR largely underestimates CC compared with observations, which should be attributed to the differences between precipitation of reanalysis products and stations. There are notable differences in different strategies within one group. For example, QMN-1 shows larger inflation when observation-based CC is higher, which is not seen in QMN-2 to 4. This is probably because QMN-1 only uses information from the one neighboring station with the highest correlation with the target station for each DOY. Higher observation-based CC in Fig. 9 means this neighboring station could be more frequently used by QMN-1 to estimate data for the target station, resulting in the larger inflation of CC. Another example is that INT-1 underestimates the CC for 68.75% stations, whereas INT-2 to 4 overestimates the CC for almost all stations. For SCD-1, inflation of CC is observed for 76.60% stations, whereas the magnitude of overestimation is

517   smaller than that in Fig. 8. The mean values of observation-based and estimate-based CC are 0.71 and 0.77,

518   respectively. SCD-2 replaces estimates by observations and is the final dataset of this study. It reduces the mean

519   estimate-based CC to 0.70. The overall spatial correlation structure of observations is generally preserved by SCD-2.

520   However, SCD-2 calculates CC for the entire period which is different from the period of observation-based CC,

521   resulting in uncertainties such as the underestimation for some stations when observation-based CC is larger than 0.7.

522   The spatial correlation of T_{min} is much stronger than that of precipitation (Fig. 10). Most strategies overestimate the

523   CC for most stations, whereas the magnitude is quite small. For example, SCD-1 inflates the CC for 96.96% stations,

524   while the mean CC values for observations (0.95) and SCD-1 (0.96) are very close to each other. QMR still

525   underestimates CC similar to Fig. 9 for precipitation. CC based on SCD-2 is generally consistent with that based on

526   observations, while slight underestimation exists for some stations when observation-based CC is higher than 0.9. T_{max}

527   shows similar spatial correlation patterns with T_{min} (Fig. S8).

528   In summary, inflation of CC is inevitable particularly when estimates are obtained using information from a sole data

529   source such as one neighboring station or one reanalysis product. The inflation is larger if each DOY is treated

530   separately (Fig. 8 and S7), but smaller if CC is calculated for all years (Fig. 9, 10 and S8). Combining information

531   from multiple sources (stations and reanalysis) and combining multiple strategies for each DOY are beneficial in

532   estimating the overall spatial correlation structure. The spatial correlation structures vary for different strategies, and

533   further studies are needed to clearly demonstrate how and why the estimate-based CC differs from observation-based

534   CC.

535
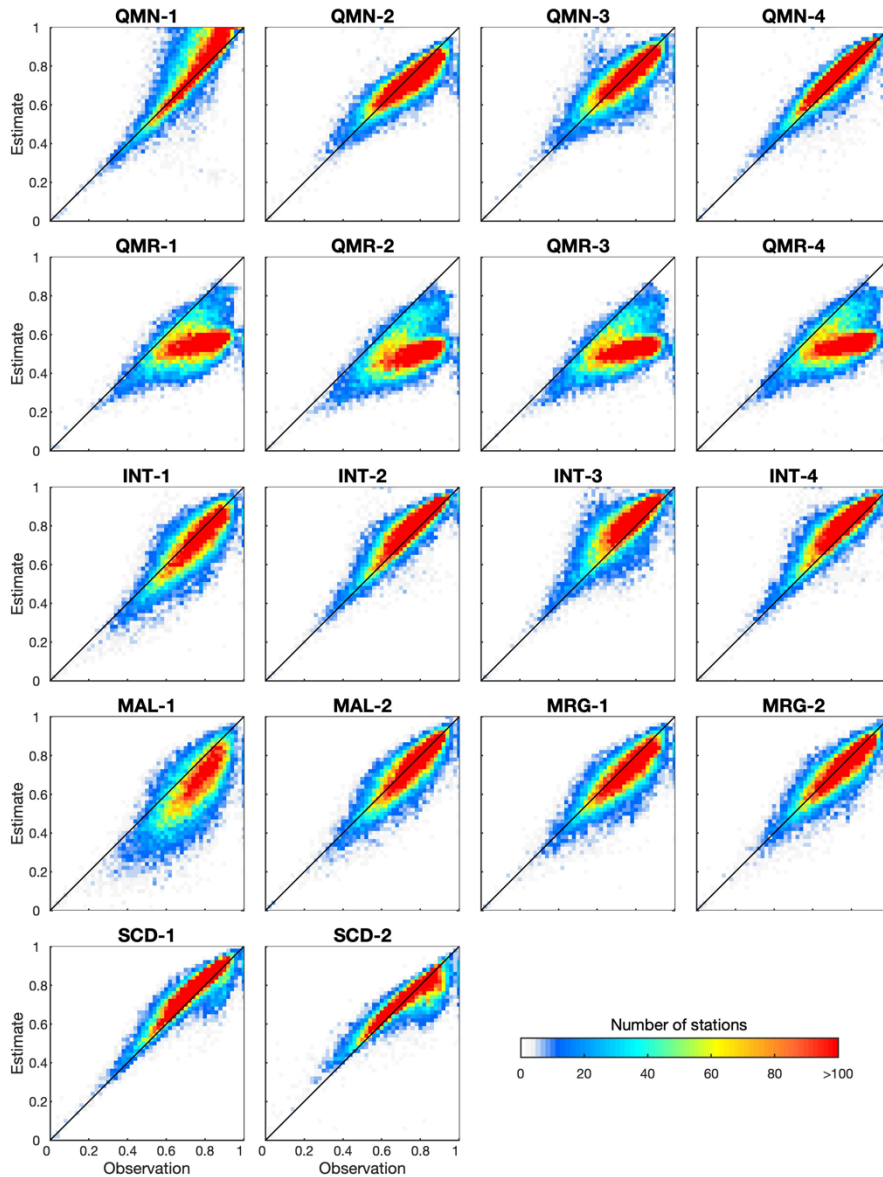
Figure 9. Scatter density plots of CC between precipitation from the target station and neighboring stations. For each target station, the neighboring station with the highest correlation with the target station is selected. X-axis represents the CC between observed precipitation from target and neighboring stations. Y-axis represents the CC between estimated precipitation from the target station and the observed precipitation from the neighboring station. Each sub-figure corresponds to one strategy in Sect. 3.3.2. SCD-1 represents SCD estimates after correction, while SCD-2 replaces estimates by observations. CC is calculated during the overlapped observation period between target and neighboring stations, and the only exception is SCD-2 which calculates CC using precipitation from target and neighboring stations during the entire period.

544
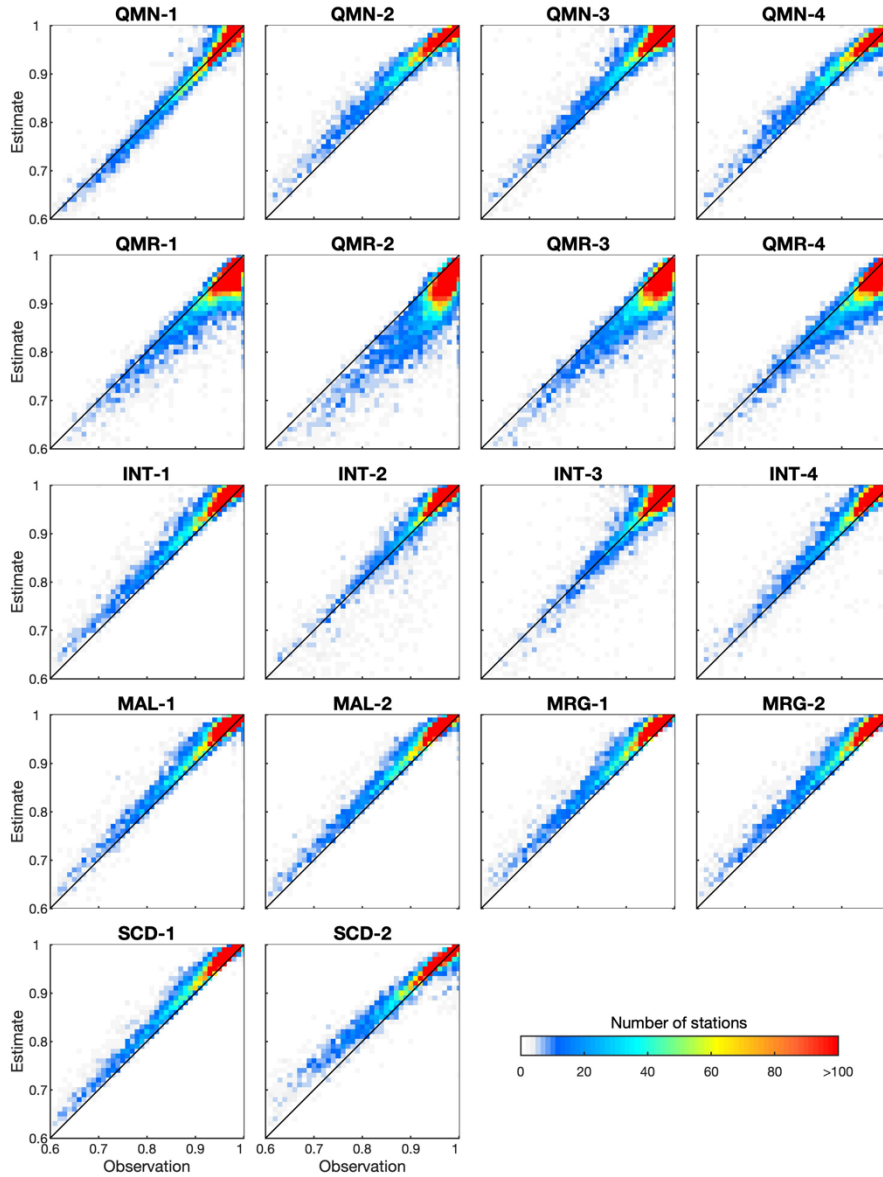
Figure 10. Similar with Fig. 9, but for T_{min}.

The variability of observations and of the corrected and uncorrected SCDNA estimates (Step-7 in Sect. 3.3.3) are compared using the standard deviation of the observation period (Fig. 11). The standard deviation of uncorrected SCDNA precipitation is lower than that of observations, while after correction, the standard deviation agrees very well with observations. The mean values of standard deviation are 7.36, 6.30, and 7.36 for observations, uncorrected SCDNA, and corrected SCDNA, respectively. For T_{min} and T_{max}, corrected and uncorrected SCDNA estimates both show consistent variability with observations.
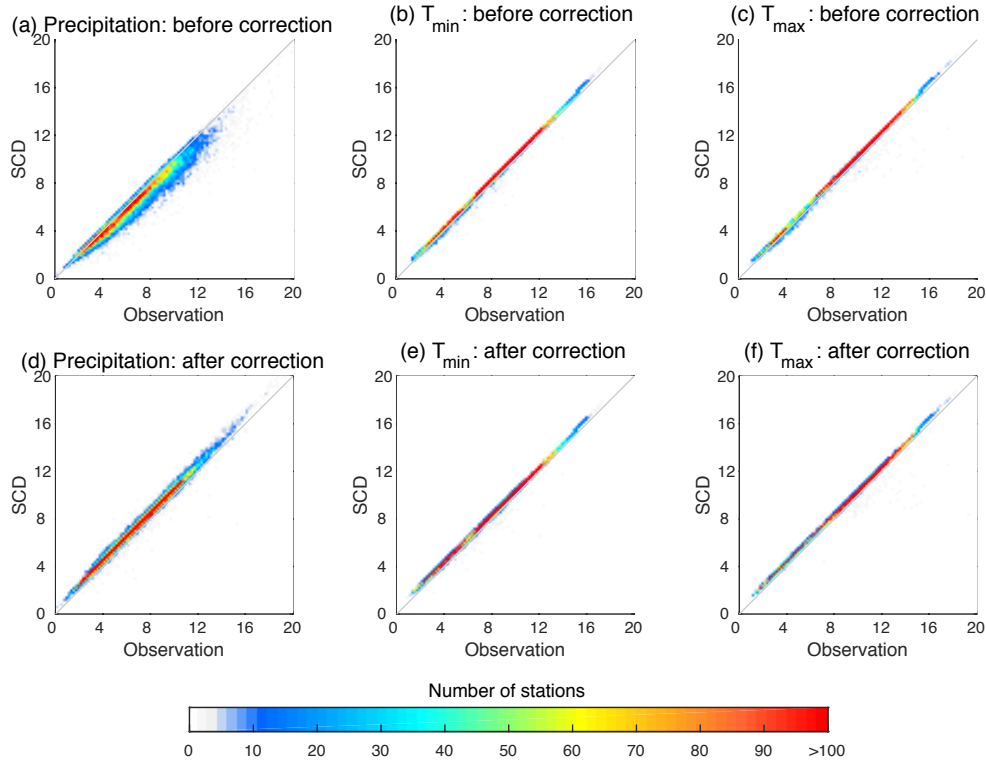
Figure 11. The standard deviation of observations and SCDNA estimates before and after correction. Data in the observation period are used.

4.3 The performance of the serially complete dataset

Uncorrected SCDNA estimates show high accuracy in North America (Fig. 12). For precipitation, the median KGE' of all stations is 0.87, and the median values of r, β, and γ are 0.91, 0.92, and 0.96, respectively. The KGE' for Mexico stations generally ranges between 0.6 and 0.8, which is smaller than that in U.S. and southern Canada. Some stations in Rocky Mountains, Caribbean, Alaska and northern Canada (regions with complex topography or climate), also show lower KGE' for precipitation estimates. The spatial distribution of r is similar with that of KGE', while the magnitude is higher. According to γ, most stations underestimate precipitation variability which is consistent with Fig. 11; β is generally lower than one in most regions of North America, particularly in the Rocky Mountains and Mexico where SCDNA underestimates precipitation.

Estimated temperature shows much higher KGE' compared with precipitation. The median KGE' and r of T_{min} are 0.97 and 0.99, respectively. For T_{max}, the median of KGE' and r are 0.99 and 0.99, respectively. The median γ and β are both between 0.99 and 1 for T_{min} and T_{max} with small variations, particularly for T_{max} (Fig. 12); the KGE' of T_{min} and T_{max} is lower in Caribbean and Mexico. For T_{min}, the KGE' for some stations around 45°N and the Rocky Mountains is lower than surrounding regions although γ is spatially homogeneous for the same region. This is because the mean T_{min} is close to zero for some stations in this region, resulting in the large magnitude of β and γ. In contrast, T_{max} exhibits homogeneous performance in the same region for all metrics.

571   Corrected SCDNA estimates (see Step-7; Fig. S9) have higher accuracy than uncorrected estimates (Fig. 12). For

572   example, the median KGE' for precipitation is improved from 0.87 to 0.90 after correction. The KGE' for T_{min} and

573   T_{max} is also improved but not as significant as precipitation. β equals to one for all stations due to the mean-value

574   correction. γ for precipitation changes from negative to positive for all stations, whereas the magnitude of bias

575   (deviation from one) is smaller after correction. As a result, the spatial distribution of metrics for T_{min} is also more

576   homogeneous.
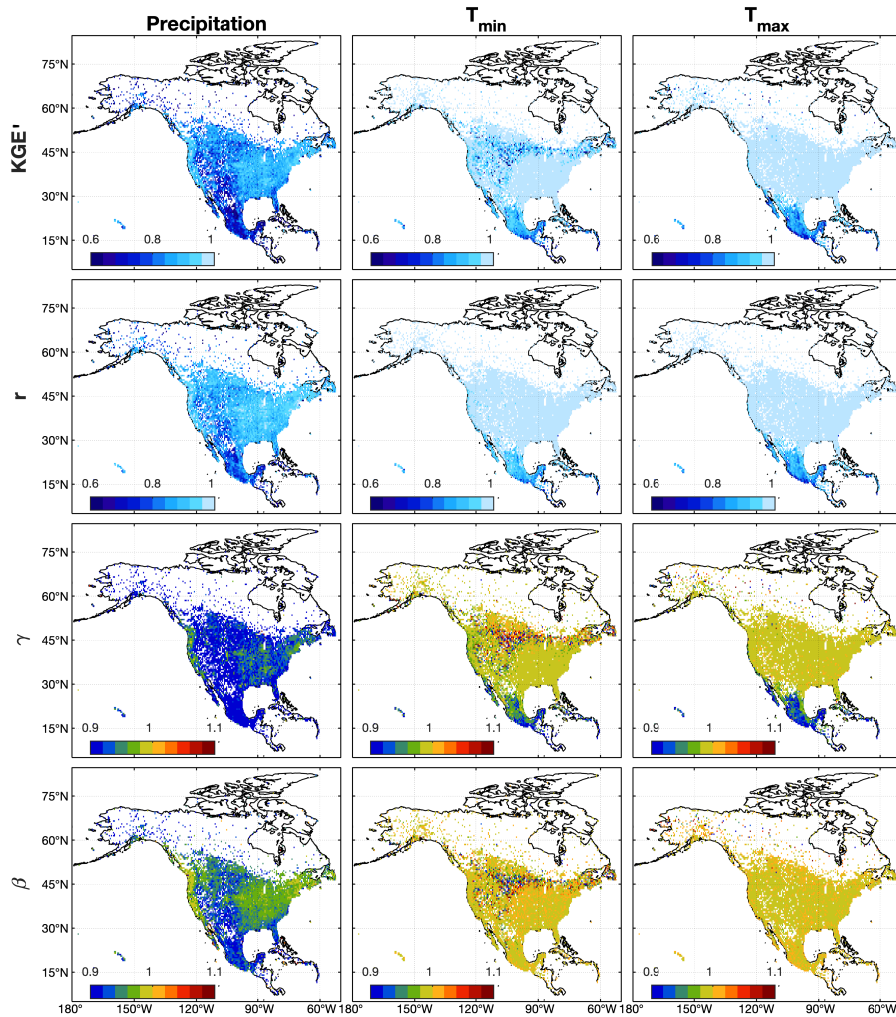
577

578   Figure 12. The spatial distributions of KGE' and its three components (r is CC, β is the bias ratio, and γ is the

579   variability ratio) for uncorrected SCDNA estimates over North America during the observation period. The maps are

580   at the resolution of 0.5°. The value for each grid cell is the median value of all stations within this grid cell.

581   The distributions of KGE' vary during the year (Fig. 13). For precipitation, more stations show lower KGE' during

582   summer (DOY 150 to 250) than at other times of the year, which may be due to the variability of summertime

583   convective precipitation. For T_{min}, some stations show lower KGE' from DOY 100 to 250. The seasonal variation of

584   KGE' for T_{max} is relatively weak, although KGE' is slightly more concentrated at a higher level during spring and

585   autumn than winter and summer. The overall performance of T_{max} is better than T_{min} and precipitation.
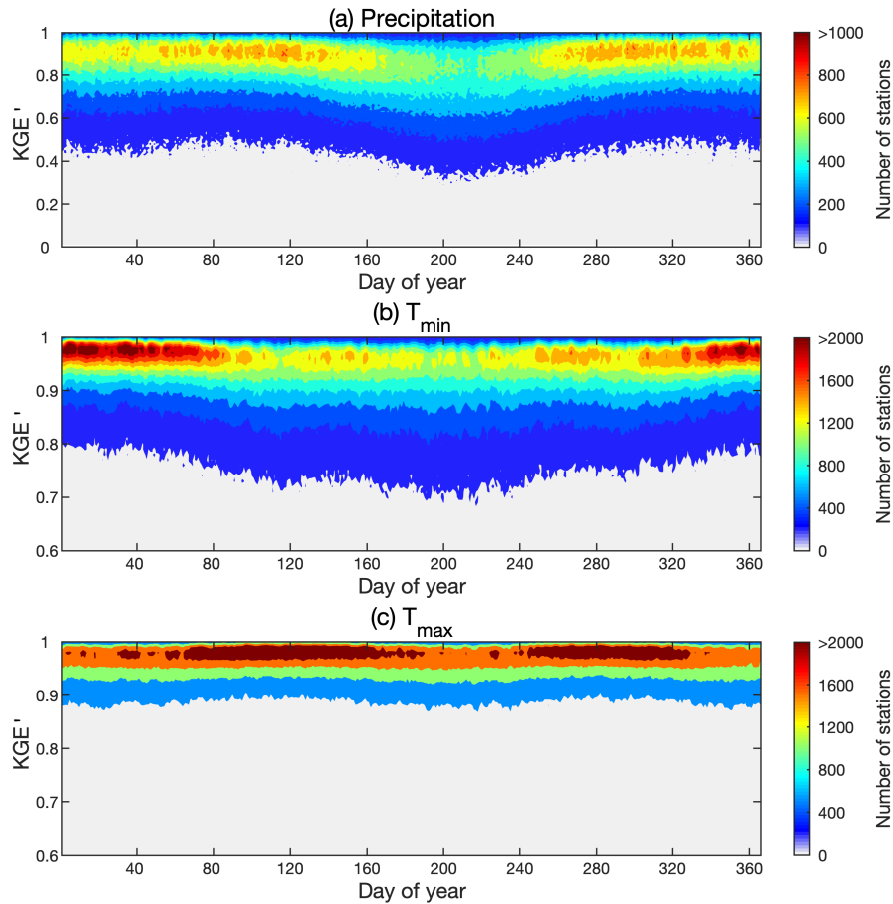
586

587   Figure 13. The distribution of KGE' for each day of year for (a) precipitation, (b) T_{min}, and (c) T_{max}. Corrected SCDNA

588   estimates are used.

589   4.4 Comparison between the serially complete dataset and gridded products

590   SCDNA precipitation and temperature are compared with benchmark gridded products to demonstrate whether the

591   SCDNA is a good choice when station data are unavailable. Actual station observations are used as reference.

592   Although assessing gridded products using point-scale station data contains uncertainties (Tang et al., 2018a), the

593   objective of this section is to illustrate their agreement with station observations in lieu of providing an exhaustive

594   quantitative assessment of their real-world accuracy.

595   Overall, the SCDNA achieves much higher KGE' than reanalysis products for all variables (Fig. 14). For precipitation,

596   the median KGE' differences between the SCDNA and ERA5, JRA-55 and MERRA-2 are 0.48, 0.57, and 0.54,

597   respectively. The corresponding KGE' differences for T_{min} are 0.46, 0.61, and 0.36, respectively. The improvement

598   for T_{max} is smaller, particularly in the eastern U.S. where the topography is relatively flatter compared with western

599   U.S. The KGE' differences of T_{mean} are lower than T_{min} but higher than T_{max} due to the offset effect. T_{range} suffers little

600   from the elevation differences between stations and reanalysis grids, and is suitable to demonstrate the differences

601   between SCDNA and reanalysis products. The median KGE' differences for T_{range} between the SCDNA and ERA5,

602   JRA-55 and MERRA-2 are 0.31, 0.48, and 0.31, respectively.
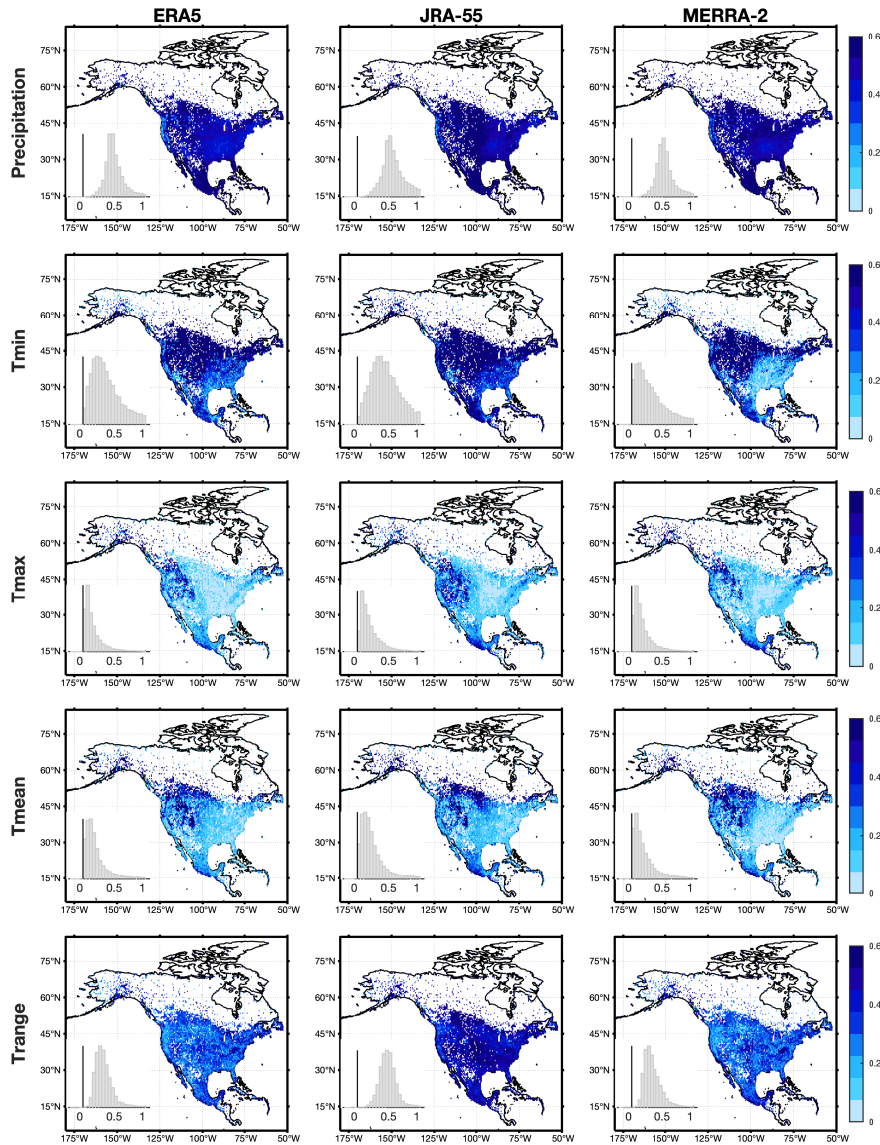
603

604   Figure 14. Spatial distributions of KGE' differences between SCDNA estimates and three reanalysis products (ERA5,

605   JRA-55, and MERRA-2). The nested histograms show KGE' differences between the SCDNA and reanalysis products.

606   Corrected SCDNA estimates are used.

607   SCDNA and MSWEP precipitation is compared (Fig. 15). Since MSWEP merges data from numerous stations, the

608   evaluation of MSWEP based on station data is not independent, which could result in the overestimation of its KGE'.

609   Even so, SCDNA precipitation shows higher KGE' than MSWEP for 98.97% stations with a median KGE' difference

610   of 0.31. Fig. 15 shows notable differences between MSWEP and SCDNA at the Canada-USA border and the USA-
611   Mexico border. This is because MSWEP infers gauge reporting time by searching for the highest correlation between
612   gauge data and the temporally shifted reanalysis/satellite estimates (Beck et al., 2019). The estimated temporal shift
613   could vary with countries, which results in distinct differences of station-based evaluation results along national
614   boundaries. The accumulation periods of station and MSWEP precipitation are inconsistent in some cases, which
615   could affect the evaluation of MSWEP (see Sect. 5.1).

616   Note that the evaluation does not indicate that the SCDNA has higher accuracy than the gridded products; rather, the
617   results show that SCDNA is a better substitute than gridded products when station observations are unavailable.
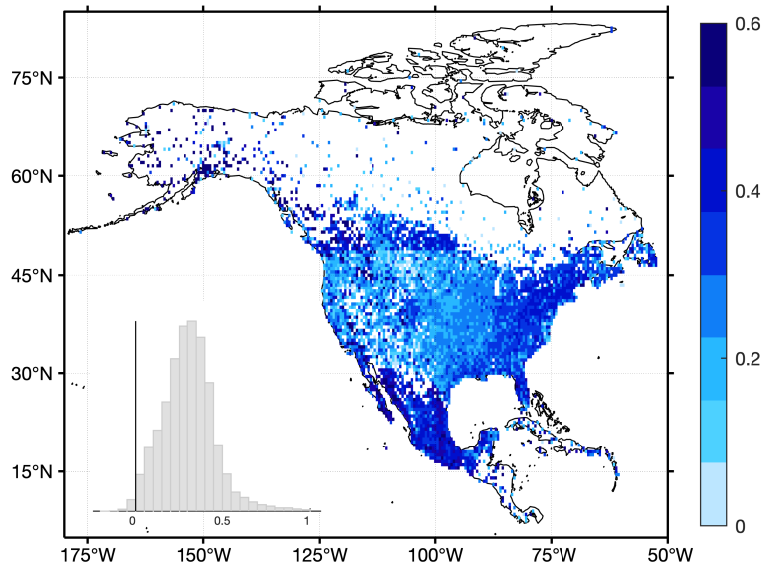
618

619   Figure 15. Spatial distributions of KGE' differences between SCDNA and MSWEP precipitation. Corrected SCDNA
620   estimates are used.

621   **5. Discussion**

622   **5.1 Observation time of stations**

623   Meteorological stations in different countries usually have different local observation time, and stations in the same
624   country may also experience change of observation time (Vincent et al., 2012). Most station databases including those
625   used in this study do not account for reporting-time inconsistencies due to lack of hourly observations and well-
626   documented station metadata. Vincent et al. (2009) examined several methods to adjust the time of daily precipitation
627   observations, which, however, often altered observed precipitation intensity. Beck et al. (2019) inferred the reporting
628   time of daily precipitation observations by calculating SCC between the series of stations and gridded products, which
629   is useful to correct the bias of gridded products. A simple experiment is carried out using the method of Beck et al.
630   (2019) to infer the lag day of station series. For precipitation, 6418 stations show nonnegligible time shift from the

631   reporting date (Fig. S10). However, this method may be unsuitable for temperature because the estimated lag day is

632   mostly zero, and the inferred reporting time cannot be directly applied to adjust station observations.

633   The inconsistent reporting time has different impact on precipitation, T_{min}, and T_{max}. For example, if a station records

634   data from 8:00 a.m. on January 1st to 8:00 a.m. on January 2nd, the station will probably use January 2nd as the

635   reporting time. However, two thirds of the 24-h time are within January 1st, indicating that the accumulated

636   precipitation could mostly occur on January 1st. T_{max} could also occur during the daytime on January 1st, but it is hard

637   to determine on which day T_{min} occurs, which makes it challenging to adjust precipitation, T_{min} and T_{max} at the same

638   time. The difference between universal and local time makes this problem more complicated. Thus, the reporting time

639   of stations is not corrected here due to aforementioned difficulties.

5.2 Homogenization

641   Inhomogeneities in station observations are defined as variations that are not caused by weather and climate factors.

642   Long-term station records are often subjected to inhomogeneities due to factors like station re-location, observation

643   time change, instrument change, and surrounding environment change (Venema et al., 2012). Many methods have

644   been developed to identify breakpoints and homogenize station series in annual, monthly or even daily scales (e.g.,

645   Ma et al., 2008; Vincent et al., 2002, 2012). Different methods could generate different estimates of inhomogeneities

646   as shown by many comparison studies (e.g., Beaulieu et al., 2008; Reeves et al., 2007; Venema et al., 2012). The four

647   station databases (Sect. 2.1) used in this study provide original station records without homogenization. The SCDNA

648   would inherit the potential inhomogeneities contained in these databases, and the infilling/reconstruction may also

649   lead to discontinuities. The homogenization of the SCDNA is challenging considering that (1) the dataset covers a

650   broad range of climate, topography, and countries, (2) the number of stations is large and differences between station

651   periods (ranging from 8 to 40 years) are substantial, and (3) whether existing methods are suitable for homogenization

652   of infilling/reconstruction estimates needs exploration. Therefore, homogenization is not carried out in this study,

653   which, however, is an important direction for future studies.

5.3 Limitations of the KGE' statistic

655   We use KGE' because it incorporates information about correlation, bias, and variability, and hence provides more

656   information on methodological performance than an individual metric. For example, the PCC between temperature

657   estimates and observations is usually close to one and cannot reflect the bias term, while the mean square error is

658   prone to the effect of extreme values (or outliers). However, KGE' also has limitations. For example, the values of

659   KGE' depend on the units of measurement (e.g., Santos et al., 2018) – in our case, the β values for temperature are

660   clearly always close to one if the units of measurement for temperature are in Kelvin. Since these statistics incorrectly

661   indicate very small temperature biases, we used °C for all KGE' calculations in this study, ensuring that β has more

662   leverage in the KGE' statistic. Moreover, and critical for our analysis, the normalization used in the KGE' formula (β

663   and γ) means that the KGE' values are low when the denominators of β and γ are close to zero (e.g., Santos et al.,

664   2018). This problem is especially acute for temperature – for instance, we found that KGE' values were very small for

665   cases where μ_o is close to zero. Nevertheless, the number of cases where μ_o is close to zero is rather small, where

666   ~0.5% of all cases (based on all stations and all DOY) show absolute values of mean T_{min} smaller than 0.1℃. For cases

667   with μ_o close to zero, the ranking based on KGE' is similar to the ranking based on mean absolute error, which

668   means that KGE' can still function as a ranking indicator when its value is low. Further work is needed to both

669   comprehensively evaluate the alternative infilling strategies presented in this paper and evaluate more advanced multi-

670   method merging strategies.

671 **5.4 Potential improvement directions**

672   Several steps could be taken to improve the SCDNA. First, the optimal strategy could be different for each station as

673   shown by the results in this study. Therefore, the quality of SCDNA may be further improved by using more

674   infilling/reconstruction methods, which would yield diminishing returns at some point. For example, the long short-

675   term memory (LSTM) could be suitable to impute missing station observations. Optimizing the configuration of

676   various strategies will be necessary to balance computation efficiency and estimation accuracy, particularly when the

677   number of stations is large. Second, some stations suffer from undercatch, which depends on gauge type, precipitation

678   phase, environmental conditions, etc. The bias caused by undercatch can be substantial for stations located in high

679   latitudes and the mountains (Yang et al., 2005; Scaff et al., 2015). Third, the SCDNA does not distinguish between

680   rainfall and snowfall. Considering that a large part of North America has frequent snowfall in winter, precipitation

681   phase classification will be useful for hydrometeorological studies. Auxiliary data from reanalysis and satellite

682   products could be used to partition precipitation into rain and snow. Finally, although the SCDNA agrees well with

683   station observations, long-term trends are difficult to reconstruct when actual observations are unavailable, meaning

684   the SCDNA may not be suitable for climate trend analysis in the reconstruction period. Some gridded datasets use

685   only stations with long-term records (e.g., (Wood, 2008; Werner et al., 2019) to achieve temporally consistent

686   estimates, whereas such stations are very few. Reasonable trend estimation is challenging but meaningful for SCD.

687   Furthermore, other variables such as wind and humidity observed by stations also suffer from the same problems faced

688   by precipitation and temperature. Future studies should explore whether the current methodology is applicable to other

689   variables. A SCD covering more variables would be useful for research in various fields.

690 **6 Data availability**

691   The SCDNA dataset is available at https://doi.org/10.5281/zenodo.3735533 (Tang et al., 2020) in netCDF format. The

692   basic variables are station identification, latitude, longitude, elevation, date, and TLR derived in Sect. 3.2. Stations

693   that undergo location merging (Sect. 3.1.1) are identified and all relevant stations are included in the data file. For

694   precipitation, T_{min}, and T_{max}, the variables in the netCDF4 file include original station observations, quality flags

695   provided by original station databases, quality flags provided by this study, estimates from 16 strategies, uncorrected

696   SCDNA estimates, corrected SCDNA estimates, the final SCDNA with estimates replaced by observations, data

697   source flags indicating the source of each record in SCDNA (observations or 16 strategies), and accuracy metrics

698   (KGE' and its three components) for all estimates (16 strategies and SCDNA).

699 Scripts used to produce the SCDNA are available at https://github.com/tgq14/GapFill. The dataset will be regularly
700 updated to cover the latest periods.

701 **7 Conclusions**

702 This study developed a daily SCD of precipitation, T_{min}, and T_{max} for 27276 stations from 1979 to 2018 over North
703 America (SCDNA). The original station data are compiled from multiple sources and undergo strict quality control.
704 Many stations have nonnegligible fractions of missing values in observation and reconstruction periods. For each
705 station, the infilling and reconstruction are implemented using 16 strategies (quantile mapping, statistical interpolation,
706 and machine learning) based on information from neighboring stations and concurrent reanalysis estimates (ERA5,
707 JRA-55, and MERRA-2). The final SCDNA combines estimates from the 16 strategies and is corrected using station
708 observations. The spatial correlation is preserved and might be slightly inflated. The SCDNA estimates reproduce the
709 variance of original station observations very well, particularly for temperature. The median KGE' of the final
710 precipitation, T_{min}, and T_{max} for all stations is 0.90, 0.98, and 0.99, respectively. The comparison with four benchmark
711 gridded products shows that the SCDNA has much better agreement with station observations. The SCDNA will be
712 useful for a variety of hydrometeorological studies in North America.

713

714 **Author contributions:** GT and MC designed the study. GT performed the analyses and wrote the paper. All authors
715 contributed to data analysis, discussions about the methods and results, and paper improvement.

716 **Competing interests:** The authors declare that they have no conflict of interest.

717 **Acknowledgements:** The study is funded by the Global Water Futures (GWF) program in Canada. The authors
718 appreciate the extensive efforts from the developers of the ground and reanalysis datasets to make their products
719 available. The authors also thank Zenodo (https://zenodo.org/) for publishing our dataset as open access to users.

720 **Appendix A**

721 Table A1. Acronyms used in this paper

Acronym	Full name
ANN	Artificial neural network
APHRODITE	Asian Precipitation-Highly-Resolved Observational Data Integration Towards Evaluation
CC	Correlation coefficient
CDF	Cumulative distribution function
CONUS	Contiguous United States
DEM	Digital elevation model

DOY	Day of year
ECCC	Environment and Climate Change Canada
ERA5	the fifth generation of ECMWF atmospheric reanalyses of the global climate
fD	Fraction of days without precipitation
GHCN-D	Global Historical Climate Network Daily
GSOD	Global Surface Summary of the Day
IDW	Inverse distance weighting
INT	Interpolation
JRA-55	Japanese 55-year Reanalysis
KGE'	Kling-Gupta Efficiency
LSTM	Long short-term memory
MAL	Machine learning
MLAD	Multiple regression based on the least absolute deviation criteria
MERIT DEM	Multi-Error-Removed Improved-Terrain digital elevation model
MERRA-2	Modern-Era Retrospective analysis for Research and Applications, Version 2
MRG	Multi-strategy merging
MSWEP	Multi-Source Weighted-Ensemble Precipitation
NR	Revised normal ratio
PCC	Pearson CC
QM	Quantile mapping
QMN	QM using neighboring stations
QMR	Quantile mapping with concurrent reanalysis estimates
RF	Random forest
SCC	Spearman CC
SCDs	Serially complete datasets
TLR	Temperature lapse rate
T_{max}	Maximum temperature
T_{mean}	Mean temperature
T_{min}	Minimum temperature
T_{range}	Daily temperature range
U.S.	United States
UTC	Universal Time Coordinated

722

Appendix B

Five types of checks (Durre et al., 2010) are adopted for the quality control of temperature.

725   1.   Integrity checks. The first type of integrity check is *a duplication check* to identify duplicated records for time
726   series in different time periods. The second type of integrity check includes *the streak check* to identify
727   consecutive identical values and *the frequent-value check* to identify close but not necessarily consecutive
728   identical values. The *world record exceedance check* sets lower (-89.4°C) and upper (57.7°C) bounds of
729   temperature.

730   2.   Outlier checks, including *the gap check* that examines the frequency distributions for all calendar months, and
731   the *climatological outlier check* that is based on the traditional z-score (e.g., Hubbard and You, 2005).

732   3.   Internal and temporal consistency checks, including *the iterative temperature consistency check*, to ensure some
733   inherent relationships are abided (e.g., T_{min} cannot be larger than T_{max}); *the spike/dip check*, identifies
734   temperatures which deviate from previous and following days by at least 25°C; and *the lagged temperature range*
735   *check*, which identifies abnormally large differences between T_{min} and T_{max} during a 3-day time window.

736   4.   Spatial consistency checks, including *the regression check* and *the spatial corroboration check. The regression*
737   *check* builds regression relationships between temperature at the target location and selected nearby stations to
738   determine whether temperature at the target station should be flagged according to regression residuals and
739   standardized residuals. *The spatial corroboration check* flags temperature at the target station if the value
740   deviates far from the temperature at neighboring stations.

741   5.   Extreme megaconsistency checks to ensure that certain relationships hold for the entire records of stations. For
742   example, T_{max} cannot be higher than the lowest T_{min} for the calendar month, and vice versa.

743 For precipitation, quality control strategies are from three studies. The first part is similar with temperature, but does
744 not include the third type of checks (internal and temporal consistency checks). The second part is from Hamada et al.
745 (2011).

746   1.   Repetition checks. The non-zero check identifies constant daily values (> 10 mm d^{-1}) that occur for more than
747   four days. The zero check compares the annual zero-precipitation frequency with its climatological value to spot
748   unusual frequencies of zero.

749   2.   Duplicated monthly or sub-monthly record check. The temporal CC and the number of days with equal
750   precipitation are used to identify whether two different months have the same records caused by human errors.

751   3.   Z-score-based outlier check. Daily precipitation is flagged if its difference with the mean value from precipitation
752   within a 15-day window of all years is larger than nine standard deviations. This step is repeated until no outlier
753   is identified.

754 4. _Spatiotemporally isolated value check_. Extremely large precipitation is identified in both space and time based
755   on the percentiles of precipitation differences between the target station and neighboring stations within a radius
756   of 400 km.

757 The third part is from Beck et al. (2019).

758 1. Empirical criterion based on the fraction of days without precipitation (fD). This was designed to identify the long
759   series of erroneous zero precipitation contained in GSOD station records. However, we found that this criterion
760   misidentifies some acceptable records in GHCN-D. Therefore, the fD-based check is only implemented for GSOD.

761 2. Discarding stations with fewer than 15 unique values or more than 99.5% dry records (<0.5 mm d^{-1}).

762 **References**

763 Alexander, L. V., Zhang, X., Peterson, T. C., Caesar, J., Gleason, B., Tank, A. M. G. K., Haylock, M., Collins, D.,
764 Trewin, B., Rahimzadeh, F., Tagipour, A., Kumar, K. R., Revadekar, J., Griffiths, G., Vincent, L., Stephenson, D. B.,
765 Burn, J., Aguilar, E., Brunet, M., Taylor, M., New, M., Zhai, P., Rusticucci, M. and Vazquez-Aguirre, J. L.: Global
766 observed changes in daily climate extremes of temperature and precipitation, J. Geophys. Res. Atmospheres, 111(D5),
767 doi:10.1029/2005JD006290, 2006.

768 Anderson, B. T., Wang, J., Salvucci, G., Gopal, S. and Islam, S.: Observed Trends in Summertime Precipitation over
769 the Southwestern United States, J. Clim., 23(7), 1937–1944, doi:10.1175/2009JCLI3317.1, 2009.

770 Beaulieu, C., Seidou, O., Ouarda, T. B. M. J., Zhang, X., Boulet, G. and Yagouti, A.: Intercomparison of
771 homogenization techniques for precipitation data, Water Resour. Res., 44(2), doi:10.1029/2006WR005615, 2008.

772 Beck, H. E., van Dijk, A. I. J. M., Levizzani, V., Schellekens, J., Miralles, D. G., Martens, B. and de Roo, A.: MSWEP:
773 3-hourly 0.25° global gridded precipitation (1979–2015) by merging gauge, satellite, and reanalysis data, Hydrol.
774 Earth Syst. Sci., 21(1), 589–615, doi:10.5194/hess-21-589-2017, 2017.

775 Beck, H. E., Wood, E. F., Pan, M., Fisher, C. K., Miralles, D. G., van Dijk, A. I. J. M., McVicar, T. R. and Adler, R.
776 F.: MSWEP V2 Global 3-Hourly 0.1° Precipitation: Methodology and Quantitative Assessment, Bull. Am. Meteorol.
777 Soc., 100(3), 473–500, doi:10.1175/BAMS-D-17-0138.1, 2019.

778 Breiman, L.: Random Forests, Mach. Learn., 45(1), 5–32, doi:10.1023/A:1010933404324, 2001.

779 Cannon, A. J., Sobie, S. R. and Murdock, T. Q.: Bias Correction of GCM Precipitation by Quantile Mapping: How
780 Well Do Methods Preserve Changes in Quantiles and Extremes?, J. Clim., 28(17), 6938–6959, doi:10.1175/JCLI-D-
781 14-00754.1, 2015.

782 Che Ghani, N. Z., Abu Hasan, Z. and Tze Liang, L.: Estimation of Missing Rainfall Data Using GEP: Case Study of
783 Raja River, Alor Setar, Kedah, Adv. Artif. Intell., doi:10.1155/2014/716398, 2014.

784 Copernicus Climate Change Service (C3S): ERA5: Fifth generation of ECMWF atmospheric reanalyses of the global
785 climate, Copernic. Clim. Change Serv. Clim. Data Store CDS Access Date July 2019 [online] Available from:
786 https://cds.climate.copernicus.eu/cdsapp#!/home, 2017.

787 Coulibaly, P. and Evora, N. D.: Comparison of neural network methods for infilling missing daily weather records, J.
788 Hydrol., 341(1), 27–41, doi:10.1016/j.jhydrol.2007.04.020, 2007.

789 Dastorani, M. T., Moghadamnia, A., Piri, J. and Rico-Ramirez, M.: Application of ANN and ANFIS models for
790 reconstructing missing flow data, Environ. Monit. Assess., 166(1), 421–434, doi:10.1007/s10661-009-1012-8, 2010.

791 Devi, U., Shekhar, M. S., Singh, G. P., Rao, N. N. and Bhatt, U. S.: Methodological application of quantile mapping
792 to generate precipitation data over Northwest Himalaya, Int. J. Climatol., 39(7), 3160–3170, doi:10.1002/joc.6008,
793 2019.

794 Devine, K. A. and Mekis, E.: Field accuracy of Canadian rain measurements, Atmosphere-Ocean, 46(2), 213–227,
795 2008.

796 Di Luzio, M., Johnson, G. L., Daly, C., Eischeid, J. K. and Arnold, J. G.: Constructing Retrospective Gridded Daily
797 Precipitation and Temperature Datasets for the Conterminous United States, J. Appl. Meteorol. Climatol., 47(2), 475–
798 497, doi:10.1175/2007JAMC1356.1, 2008.

799 Di Piazza, A., Conti, F. L., Noto, L. V., Viola, F. and La Loggia, G.: Comparative analysis of different techniques for
800 spatial interpolation of rainfall data to create a serially complete monthly time series of precipitation for Sicily, Italy,
801 Int. J. Appl. Earth Obs. Geoinformation, 13(3), 396–408, doi:10.1016/j.jag.2011.01.005, 2011.

802 Durre, I., Menne, M. J., Gleason, B. E., Houston, T. G. and Vose, R. S.: Comprehensive Automated Quality Assurance
803 of Daily Surface Observations, J. Appl. Meteorol. Climatol., 49(8), 1615–1633, doi:10.1175/2010JAMC2375.1, 2010.

804 Eischeid, J. K., Bruce Baker, C., Karl, T. R. and Diaz, H. F.: The Quality Control of Long-Term Climatological Data
805 Using Objective Data Analysis, J. Appl. Meteorol., 34(12), 2787–2795, doi:10.1175/1520-
806 0450(1995)034<2787:TQCOLT>2.0.CO;2, 1995.

807 Eischeid, J. K., Pasteris, P. A., Diaz, H. F., Plantico, M. S. and Lott, N. J.: Creating a Serially Complete, National
808 Daily Time Series of Temperature and Precipitation for the Western United States, J. Appl. Meteorol., 39(9), 1580–
809 1591, doi:10.1175/1520-0450(2000)039<1580:CASCND>2.0.CO;2, 2000.

810 Gao, L., Bernhardt, M. and Schulz, K.: Elevation correction of ERA-Interim temperature data in complex terrain,
811 Hydrol. Earth Syst. Sci., 16(12), 4661–4673, doi:10.5194/hess-16-4661-2012, 2012.

812 Gao, L., Wei, J., Wang, L., Bernhardt, M., Schulz, K. and Chen, X.: A high-resolution air temperature data set for the
813 Chinese Tian Shan in 1979–2016, Earth Syst. Sci. Data, 10(4), 2097–2114, doi:10.5194/essd-10-2097-2018, 2018.

814 Gardner, A. S., Sharp, M. J., Koerner, R. M., Labine, C., Boon, S., Marshall, S. J., Burgess, D. O. and Lewis, D.:
815 Near-Surface Temperature Lapse Rates over Arctic Glaciers and Their Implications for Temperature Downscaling, J.
816 Clim., 22(16), 4281–4298, doi:10.1175/2009jcli2845.1, 2009.

817 Gelaro, R., McCarty, W., Suárez, M. J., Todling, R., Molod, A., Takacs, L., Randles, C. A., Darmenov, A., Bosilovich,
818 M. G., Reichle, R., Wargan, K., Coy, L., Cullather, R., Draper, C., Akella, S., Buchard, V., Conaty, A., da Silva, A.
819 M., Gu, W., Kim, G.-K., Koster, R., Lucchesi, R., Merkova, D., Nielsen, J. E., Partyka, G., Pawson, S., Putman, W.,
820 Rienecker, M., Schubert, S. D., Sienkiewicz, M. and Zhao, B.: The Modern-Era Retrospective Analysis for Research
821 and Applications, Version 2 (MERRA-2), J. Clim., 30(14), 5419–5454, doi:10.1175/jcli-d-16-0758.1, 2017.

822 Gruber, S.: Derivation and analysis of a high-resolution estimate of global permafrost zonation, The Cryosphere, 6(1),
823 221–233, doi:10.5194/tc-6-221-2012, 2012.

824 Gupta, H. V., Kling, H., Yilmaz, K. K. and Martinez, G. F.: Decomposition of the mean squared error and NSE
825 performance criteria: Implications for improving hydrological modelling, J. Hydrol., 377(1–2), 80–91, 2009.

826 Hamada, A., Arakawa, O. and Yatagai, A.: An Automated Quality Control Method for Daily Rain-gauge Data, Glob.
827 Environ. Res., 15(2), 183–192, 2011.

828 Hasanpour Kashani, M. and Dinpashoh, Y.: Evaluation of efficiency of different estimation methods for missing
829 climatological data, Stoch. Environ. Res. Risk Assess., 26(1), 59–71, doi:10.1007/s00477-011-0536-y, 2012.

830 Hubbard, K. G. and You, J.: Sensitivity Analysis of Quality Assurance Using the Spatial Regression Approach—A
831 Case Study of the Maximum/Minimum Air Temperature, J. Atmospheric Ocean. Technol., 22(10), 1520–1530,
832 doi:10.1175/JTECH1790.1, 2005.

833 Kanda, N., Negi, H. S., Rishi, M. S. and Shekhar, M. S.: Performance of various techniques in estimating missing
834 climatological data over snowbound mountainous areas of Karakoram Himalaya, Meteorol. Appl., 25(3), 337–349,
835 doi:10.1002/met.1699, 2018.

836 Kemp, W. P., Burnell, D. G., Everson, D. O. and Thomson, A. J.: Estimating Missing Daily Maximum and Minimum
837 Temperatures, J. Clim. Appl. Meteorol., 22(9), 1587–1593, doi:10.1175/1520-
838 0450(1983)022<1587:EMDMAM>2.0.CO;2, 1983.

839 Kenawy, A. E., López-Moreno, J. I., Stepanek, P. and Vicente-Serrano, S. M.: An assessment of the role of
840 homogenization protocol in the performance of daily temperature series and trends: application to northeastern Spain,
841 Int. J. Climatol., 33(1), 87–108, doi:10.1002/joc.3410, 2013.

842 Kling, H., Fuchs, M. and Paulin, M.: Runoff conditions in the upper Danube basin under an ensemble of climate
843 change scenarios, J. Hydrol., 424, 264–277, 2012.

844 Knowles, N., Dettinger, M. D. and Cayan, D. R.: Trends in Snowfall versus Rainfall in the Western United States, J.
845 Clim., 19(18), 4545–4559, doi:10.1175/JCLI3850.1, 2006.

846 Kobayashi, S., Ota, Y., Harada, Y., Ebita, A., Moriya, M., Onoda, H., Onogi, K., Kamahori, H., Kobayashi, C., Endo,
847 H., Miyaoka, K. and Takahashi, K.: The JRA-55 Reanalysis: General Specifications and Basic Characteristics, J.
848 Meteorol. Soc. Jpn. Ser II, 93(1), 5–48, doi:10.2151/jmsj.2015-001, 2015.

849 Livneh, B., Bohn, T. J., Pierce, D. W., Munoz-Arriola, F., Nijssen, B., Vose, R., Cayan, D. R. and Brekke, L.: A
850 spatially comprehensive, hydrometeorological data set for Mexico, the U.S., and Southern Canada 1950–2013, Sci.
851 Data, 2(1), 150042, doi:10.1038/sdata.2015.42, 2015.

852 Longman, R. J., Frazier, A. G., Newman, A. J., Giambelluca, T. W., Schanzenbach, D., Kagawa-Viviani, A., Needham,
853 H., Arnold, J. R. and Clark, M. P.: High-Resolution Gridded Daily Rainfall and Temperature for the Hawaiian Islands
854 (1990–2014), J. Hydrometeorol., 20(3), 489–508, doi:10.1175/JHM-D-18-0112.1, 2019.

855 Longman, R. J., Newman, A. J., Giambelluca, T. W. and Lucas, M.: Characterizing the Uncertainty and Assessing the
856 Value of Gap-Filled Daily Rainfall Data in Hawaii, J. Appl. Meteorol. Climatol., 59(7), 1261–1276,
857 doi:10.1175/JAMC-D-20-0007.1, 2020.

858 Ma, C., Fassnacht, S. R. and Kampf, S. K.: How Temperature Sensor Change Affects Warming Trends and Modeling:
859 An Evaluation Across the State of Colorado, Water Resour. Res., 55(11), 9748–9764, 2019.

860 Ma, L., Zhang, T., Li, Q., Frauenfeld, O. W. and Qin, D.: Evaluation of ERA-40, NCEP-1, and NCEP-2 reanalysis air
861 temperatures with ground-based measurements in China, J. Geophys. Res., 113(D15), doi:10.1029/2007jd009549,
862 2008.

863 Ma, Y., Hong, Y., Chen, Y., Yang, Y., Tang, G., Yao, Y., Long, D., Li, C., Han, Z. and Liu, R.: Performance of
864 Optimally Merged Multisatellite Precipitation Products Using the Dynamic Bayesian Model Averaging Scheme Over
865 the Tibetan Plateau, J. Geophys. Res. Atmospheres, 123(2), 814–834, doi:10.1002/2017jd026648, 2018.

866 Maraun, D.: Bias Correction, Quantile Mapping, and Downscaling: Revisiting the Inflation Issue, J. Clim., 26(6),
867 2137–2143, doi:10.1175/JCLI-D-12-00821.1, 2013.

868 Marshall, S. J., Sharp, M. J., Burgess, D. O. and Anslow, F. S.: Near-surface-temperature lapse rates on the Prince of
869 Wales Icefield, Ellesmere Island, Canada: implications for regional downscaling of temperature, Int. J. Climatol.,
870 27(3), 385–398, doi:10.1002/joc.1396, 2007.

871 Mekis, É. and Brown, R.: Derivation of an adjustment factor map for the estimation of the water equivalent of snowfall
872 from ruler measurements in Canada, Atmosphere-Ocean, 48(4), 284–293, doi:10.3137/AO1104.2010, 2010.

873 Menne, M. J., Durre, I., Vose, R. S., Gleason, B. E. and Houston, T. G.: An overview of the global historical
874 climatology network-daily database, J. Atmospheric Ocean. Technol., doi:10.1175/JTECH-D-11-00103.1, 2012.

875 Metcalfe, J. R., Routledge, B. and Devine, K.: Rainfall measurement in Canada: changing observational methodsand
876 archive adjustment procedures, J. Clim., 10(1), 92–101, 1997.

877 Minder, J. R., Mote, P. W. and Lundquist, J. D.: Surface temperature lapse rates over complex terrain: Lessons from
878 the Cascade Mountains, J. Geophys. Res., 115(D14), doi:10.1029/2009jd013493, 2010.

879 Newman, A. J., Clark, M. P., Craig, J., Nijssen, B., Wood, A., Gutmann, E., Mizukami, N., Brekke, L. and Arnold, J.
880 R.: Gridded Ensemble Precipitation and Temperature Estimates for the Contiguous United States, J. Hydrometeorol.,
881 16(6), 2481–2500, doi:10.1175/JHM-D-15-0026.1, 2015.

882 Newman, A. J., Clark, M. P., Longman, R. J., Gilleland, E., Giambelluca, T. W. and Arnold, J. R.: Use of Daily Station
883 Observations to Produce High-Resolution Gridded Probabilistic Precipitation and Temperature Time Series for the
884 Hawaiian Islands, J. Hydrometeorol., 20(3), 509–529, doi:10.1175/JHM-D-18-0113.1, 2019.

885 Papalexiou, S. M. and Montanari, A.: Global and regional increase of precipitation extremes under global warming,
886 Water Resour. Res., 55(6), 4901–4914, 2019.

887 Papalexiou, S. M., AghaKouchak, A., Trenberth, K. E. and Foufoula-Georgiou, E.: Global, regional, and megacity
888 trends in the highest temperature of the year: Diagnostics and evidence for accelerating trends, Earths Future, 6(1),
889 71–79, 2018.

890 Pappas, C., Papalexiou, S. M. and Koutsoyiannis, D.: A quick gap filling of missing hydrometeorological data, J.
891 Geophys. Res. Atmospheres, 119(15), 9290–9300, 2014.

892 Paulhus, J. L. H. and Kohler, M. A.: Interpolation of missing precipitation records, Mon. Weather Rev., 80(8), 129–
893 133, doi:10.1175/1520-0493(1952)080<0129:IOMPR>2.0.CO;2, 1952.

894 Pielke Sr, R., Nielsen-Gammon, J., Davey, C., Angel, J., Bliss, O., Doesken, N., Cai, M., Fall, S., Niyogi, D. and
895 Gallo, K.: Documentation of uncertainties and biases associated with surface temperature measurement sites for
896 climate change assessment, Bull. Am. Meteorol. Soc., 88(6), 913–928, 2007.

897 Ramos-Calzado, P., Gómez-Camacho, J., Pérez-Bernal, F. and Pita-López, M. F.: A novel approach to precipitation
898 series completion in climatological datasets: application to Andalusia, Int. J. Climatol., 28(11), 1525–1534,
899 doi:10.1002/joc.1657, 2008.

900 Reeves, J., Chen, J., Wang, X. L., Lund, R. and Lu, Q. Q.: A Review and Comparison of Changepoint Detection
901 Techniques for Climate Data, J. Appl. Meteorol. Climatol., 46(6), 900–915, doi:10.1175/JAM2493.1, 2007.

902 Rubin, D. B.: Inference and missing data, Biometrika, 63(3), 581–592, doi:10.1093/biomet/63.3.581, 1976.

903 Santos, L., Thirel, G. and Perrin, C.: Technical note: Pitfalls in using log-transformed flows within the KGE criterion,
904 Hydrol. Earth Syst. Sci., 22, 4583–4591, doi:10.5194/hess-22-4583-2018, 2018.

905 Sattari, M.-T., Rezazadeh-Joudi, A. and Kusiak, A.: Assessment of different methods for estimation of missing data
906 in precipitation studies, Hydrol. Res., 48(4), 1032–1044, doi:10.2166/nh.2016.364, 2017.

907 Scaff, L., Yang, D., Li, Y. and Mekis, E.: Inconsistency in precipitation measurements across the Alaska–Yukon
908 border, The Cryosphere, 9(6), 2417–2428, doi:10.5194/tc-9-2417-2015, 2015.

909 Serrano-Notivoli, R., Beguería, S. and Luis, M. de: STEAD: a high-resolution daily gridded temperature dataset for
910 Spain, Earth Syst. Sci. Data, 11(3), 1171–1188, doi:https://doi.org/10.5194/essd-11-1171-2019, 2019.

911 Shepard, D.: A two-dimensional interpolation function for irregularly-spaced data, in Proceedings of the 1968 23rd
912 ACM national conference, pp. 517–524, ACM., 1968.

913 Simolo, C., Brunetti, M., Maugeri, M. and Nanni, T.: Improving estimation of missing values in daily precipitation
914 series by a probability density function-preserving approach, Int. J. Climatol., 30(10), 1564–1576,
915 doi:10.1002/joc.1992, 2010.

916 Stooksbury, D. E., Idso, C. D. and Hubbard, K. G.: The Effects of Data Gaps on the Calculated Monthly Mean
917 Maximum and Minimum Temperatures in the Continental United States: A Spatial and Temporal Study, J. Clim.,
918 12(5), 1524–1533, doi:10.1175/1520-0442(1999)012<1524:TEODGO>2.0.CO;2, 1999.

919 Tang, G., Behrangi, A., Long, D., Li, C. and Hong, Y.: Accounting for spatiotemporal errors of gauges: A critical step
920 to evaluate gridded precipitation products, J. Hydrol., 559, 294–306, doi:10.1016/j.jhydrol.2018.02.057, 2018a.

921 Tang, G., Behrangi, A., Ma, Z., Long, D. and Hong, Y.: Downscaling of ERA-Interim Temperature in the Contiguous
922 United States and Its Implications for Rain–Snow Partitioning, J. Hydrometeorol., 19(7), 1215–1233,
923 doi:10.1175/jhm-d-18-0041.1, 2018b.

924 Tang, G., Clark, M. P., Newman, A. J., Wood, A. W., Papalexiou, S. M., Vionnet, V., Whitfield, P. H.: SCDNA: a
925 serially complete precipitation and temperature dataset for North America from 1979 to 2018 [Dataset], Zenodo,
926 https://doi.org/10.5281/zenodo.3735533, 2020.

928 Tang, Q., Wood, A. W. and Lettenmaier, D. P.: Real-Time Precipitation Estimation Based on Index Station Percentiles,
929 J. Hydrometeorol., 10(1), 266–277, doi:10.1175/2008JHM1017.1, 2009.

930 Teegavarapu, R. S. V. and Chandramouli, V.: Improved weighting methods, deterministic and stochastic data-driven
931 models for estimation of missing precipitation records, J. Hydrol., 312(1), 191–206,
932 doi:10.1016/j.jhydrol.2005.02.015, 2005.

933 Ustaoglu, B., Cigizoglu, H. K. and Karaca, M.: Forecast of daily mean, maximum and minimum temperature time
934 series by three artificial neural network methods, Meteorol. Appl., 15(4), 431–445, doi:10.1002/met.83, 2008.

935 Venema, V. K. C., Mestre, O., Aguilar, E., Auer, I., Guijarro, J. A., Domonkos, P., Vertacnik, G., Szentimrey, T.,
936 Stepanek, P., Zahradnicek, P., Viarre, J., Müller-Westermeier, G., Lakatos, M., Williams, C. N., Menne, M. J., Lindau,
937 R., Rasol, D., Rustemeier, E., Kolokythas, K., Marinova, T., Andresen, L., Acquaotta, F., Fratianni, S., Cheval, S.,
938 Klancar, M., Brunetti, M., Gruber, C., Prohom Duran, M., Likso, T., Esteban, P. and Brandsma, T.: Benchmarking
939 homogenization algorithms for monthly data, Clim. Past, 8(1), 89–115, doi:10.5194/cp-8-89-2012, 2012.

940 Vicente-Serrano, S. M., Saz-Sanchez, M. A. and Cuadrat, J. M.: Comparative analysis of interpolation methods in the
941 middle Ebro Valley (Spain): application to annual precipitation and temperature, Clim. Res., 24(2), 161–180, doi:DOI
942 10.3354/cr024161, 2003.

943 Vincent, L. A., Zhang, X., Bonsal, B. R. and Hogg, W. D.: Homogenization of Daily Temperatures over Canada, J.
944 Clim., 15(11), 1322–1334, doi:10.1175/1520-0442(2002)015<1322:HODTOC>2.0.CO;2, 2002.

945 Vincent, L. A., Milewska, E. J., Hopkinson, R. and Malone, L.: Bias in Minimum Temperature Introduced by a
946 Redefinition of the Climatological Day at the Canadian Synoptic Stations, J. Appl. Meteorol. Climatol., 48(10), 2160–
947 2168, doi:10.1175/2009JAMC2191.1, 2009.

948 Vincent, L. A., Wang, X. L., Milewska, E. J., Wan, H., Yang, F. and Swail, V.: A second generation of homogenized
949 Canadian monthly surface air temperature for climate trend analysis, J. Geophys. Res. Atmospheres, 117(D18),
950 doi:10.1029/2012JD017859, 2012.

951 Wambua, R. M., Mutua, B. M. and Raude, J. M.: Prediction of Missing Hydro-Meteorological Data Series Using
952 Artificial Neural Networks (ANN) for Upper Tana River Basin, Kenya, Am. J. Water Resour., 4(2), 35–43,
953 doi:10.12691/ajwr-4-2-2, 2016.

954 Wang, X. L., Xu, H., Qian, B., Feng, Y. and Mekis, E.: Adjusted daily rainfall and snowfall data for Canada,
955 Atmosphere-Ocean, 55(3), 155–168, 2017.

956 Werner, A. T., Schnorbus, M. A., Shrestha, R. R., Cannon, A. J., Zwiers, F. W., Dayon, G. and Anslow, F.: A long-
957 term, temporally consistent, gridded daily meteorological dataset for northwestern North America, Sci. Data, 6(1), 1–
958 16, doi:10.1038/sdata.2018.299, 2019.

959 Whitfield, P. H.: Climate Station Analysis and Fitness for Purpose Assessment of 3053600 Kananaskis, Alberta,
960 Atmosphere-Ocean, 52(5), 363–383, doi:10.1080/07055900.2014.946388, 2014.

961 Woldesenbet, T. A., Elagib, N. A., Ribbe, L. and Heinrich, J.: Gap filling and homogenization of climatological
962 datasets in the headwater region of the Upper Blue Nile Basin, Ethiopia, Int. J. Climatol., 37(4), 2122–2140,
963 doi:10.1002/joc.4839, 2017.

964 Wood, A. W.: The University of Washington Surface Water Monitor: An experimental platform for national
965 hydrologic assessment and prediction, in 22nd Conf. on Hydrology., 2008.

966 Yamazaki, D., Ikeshima, D., Tawatari, R., Yamaguchi, T., O'Loughlin, F., Neal, J. C., Sampson, C. C., Kanae, S. and
967 Bates, P. D.: A high-accuracy map of global terrain elevations, Geophys. Res. Lett., 44(11), 5844–5853,
968 doi:10.1002/2017GL072874, 2017.

969 Yang, D., Kane, D., Zhang, Z., Legates, D. and Goodison, B.: Bias corrections of long-term (1973-2004) daily
970 precipitation data over the northern regions, Geophys. Res. Lett., 32(19), n/a-n/a, doi:10.1029/2005gl024057, 2005.

971 Yatagai, A., Kamiguchi, K., Arakawa, O., Hamada, A., Yasutomi, N. and Kitoh, A.: APHRODITE: Constructing a
972 Long-Term Daily Gridded Precipitation Dataset for Asia Based on a Dense Network of Rain Gauges, Bull. Am.
973 Meteorol. Soc., 93(9), 1401–1415, doi:10.1175/bams-d-11-00122.1, 2012.

974 Young, K. C.: A Three-Way Model for Interpolating for Monthly Precipitation Values, Mon. Weather Rev., 120(11),
975 2561–2569, doi:10.1175/1520-0493(1992)120<2561:ATWMFI>2.0.CO;2, 1992.

976